East European Journal of Physics. 3. 115-130 (2025)
DOI:10.26565/2312-4334-2025-3-11 ISSN 2312-4334

MODELLING OF MHD MICROPOLAR NANO FLUID FLOW IN AN INCLINED POROUS STENOSED ARTERY WITH DILATATION

Narender Satwai[a,b], Karanamu Maruthi Prasad[a]*
[a]*Department of Mathematics, School of Science, GITAM (Deemed to be University), Hyderabad, Telangana State, India–502329*
[b]*Department of Mathematics, B V Raju Institute of Technology, Vishnupur, Narsapur, Telangana State, India-502313*
**Corresponding author e-mail: mkaranam@gitam.edu*
Received April 20, 2025; revised June 1, 2025; Accepted June 9, 2025

In this paper, the impact of a magnetic field on blood flow with nanofluid particles through an inclined porous stenosed artery and dilatation was studied. Here blood is treated as micropolar fluid. The equations are solved by using Homotopy perturbation method [HPM] under the assumption of mild stenosis. The closed form solutions of velocity, temperature profile, and concentration distribution are obtained. The effects of pertinent parameters on flow phenomena have been observed and results are analyzed graphically. This study examines the impact of the magnetic parameter on flow characteristics and reveals that the presence of a magnetic field increases resistance to the flow while decreasing shear stress at the wall. A result is found that the flow resistance and shear stress at the wall decreased for heights of the stenosis dilatation. Additionally, the study finds that resistance to the flow increases and shear stress at the wall decreases with viscosity. The stream lines are drawn to examine the flow pattern and properties of momentum transfer.
Keywords: *Stenosis; Dilatation; Micropolar fluid; Flow resistance; Wall shear stress; Brownian motion parameter; Thermophoresis parameter*
PACS: 47.15.-x, 47.63.-b, 47.63.Cb

1. INTRODUCTION

Atherosclerosis, which is the narrowing of the blood vessel lumen, or the inner open space or lumen of an artery, due to fatty substance formation, is one of the most dangerous health risks in the modern world. This may result in hypertension, myocardial infarction, and further complications. Consequently, stenosis occurs when abnormal and irregular growth impedes normal blood circulation, with significant research indicating that hydrodynamic characteristics, including wall shear and flow resistance, contribute to the onset and progression of this medical condition. A comprehensive understanding of the blood flow dynamics in a stenosed vessel would facilitate precise diagnosis and treatment of cardiovascular conditions.

As a result, several researchers have explored mathematical models for confined duct flows [1,2,3,4,5]. All these mathematical analyses have characterized blood as a Newtonian fluid. Moreover, when the diameters of the artery or tube are small and the shear rate is low, blood demonstrates non-Newtonian behavior. The quantity of red blood cells (RBCs) in erythrocytes affects this behavior. Young D. F., Tsai F. Y., and P. Chaturani and R. P. Samy [6,4] conducted theoretical and experimental investigations on blood flow in arteries exhibiting mild stenosis. All these investigations aim to elucidate how stenosis influences the properties of blood flow, encompassing velocity profile, wall shear stress, and resistive impedance. Prasad K.M. and Yasa P.R. [7] developed a mathematical explanation for the flow of a micropolar fluid within a tapering stenosed artery including porous walls.

However, all these investigations concentrated on the effects of individual arterial stenosis assuming a uniform cross-section of the tube. It is acknowledged that many blood arteries display small changes in cross-section over their length and can develop multiple segments, especially at bends and junctions (Schneck et al. [8]). Addressing this complexity, Maruthi Prasad, and Radhakrishnamacharya [9] investigated blood flow in arteries with multiple stenoses and a non-uniform cross-section, modeling blood as a Herschel-Bulkley fluid.

A Cemal Eringen's [10] described simple microfluids as concentrated suspensions of neutrally buoyant deformable particles in a viscous fluid, in which the individuality of substructures influences the physical outcome of the flow. Such fluid models can be used to rheologically characterize polymeric suspensions and normal human blood, and they have been used to physiological and technical concerns Micropolar fluids are a subclass of microfluids characterized by rigid fluid microelements. Basically, these fluids may support couple strains and body couples while also exhibiting micro rotational and micro inertial effects. The fundamental benefit of using a micropolar fluid model to analyze blood flow in comparison to other types of non-Newtonian fluids is that it takes care of the rotation of fluid particles by means of an independent kinematic vector known as the microrotation vector. G. R. Charya [11] described blood flow as micropolar fluid flow through a constricted channel. Fluid circulation in a non-symmetric vessel with continuous, constrained borders is investigated in this paper. Theoretical velocity profiles are calculated using the micropolar fluid to simulate blood flow in small arteries, and the results show good agreement with the experimental data. Ariman et al. [12] presented a comprehensive examination of microcontinum fluid mechanics, illustrating numerous applications in physiological phenomena. Prasad, K. M. et al. [13] examined a mathematical explanation for two-layered fluid flow through a stenotic

Cite as: N. Satwai, K.M. Prasad, East Eur. J. Phys. 3, 115 (2025), https://doi.org/10.26565/2312-4334-2025-3-11

artery, in which the core region contains a micropolar fluid with nanoparticles, acting as a non-Newtonian fluid, while the peripheral region behaves as a Newtonian fluid. Srinivasacharya, D, et al. [14] studied the peristalsis of a micropolar fluid in a tube. Prasad, K. M. & Yasa, P. R. [15] examined the micropolar fluid flow through a permeable artery.

Blood is appropriately described as a micropolar fluid due to its complicated and changeable rheological behaviour, which is heavily influenced by changes in artery diameter. As arteries contract, microelements like red blood cells (RBCs) become compressed, increasing collision impacts and frictional interactions. These microstructural dynamics have a major effect on the viscosity and velocity profiles of blood flow [16]. Furthermore, the formation of cholesterol plaques over time can constrict the carotid artery, increasing the risk of stroke or temporary vision loss caused by disturbed or misdirected blood flow. Because plaque development and progression are controlled by local flow conditions, a micropolar fluid model is appropriate for illustrating blood's crucial micro rotational and shear-dependent behaviour in such pathological conditions [17].

Fluids that contain nanoparticles, which are incredibly tiny particles with a nanometer scale, are known as nanofluids. Nano-fluids have generated significant interest from researchers because of their increased thermal conductivity, a concept first introduced by Choi [18]. Nadeem and Noreen Sher Akbar [19] studied the flow of a micro-polar fluid infused with nanoparticles in the smaller intestine. Many researchers focused on this field because of its significance in the biomedical field [20,21,22]. Maruthi Prasad and Prabhakar Reddy [23] studied the thermal effects of two immiscible fluids within a permeable stenosed artery having Newtonian fluid in the peripheral region and a nano-fluid in the core region. Prasad, K. M. et al. [24] explored a mathematical model peristaltic pumping of Jeffrey model with nanoparticles in an inclined tube. Dawood, A. S. et al. [25] investigates nanofluid behavior in stenosed arteries by introducing a variable pressure gradient and analyzing the impact of magnetic fields on nano-blood flow. The presence of nanoparticles suspended in the base fluid is insufficient to improve thermal conductivity, as this enhancement is contingent upon the particles' shape and size of the particles.

In the human vascular system, magnetic fields are essential for controlling blood flow. Magnetohydrodynamic (MHD) applications have been demonstrated to lower blood artery fluid flow rates and aid in the treatment of cardiovascular diseases. Numerous biological uses, including drug administration, cell separation, and cancer treatment, have led to the development of magnetic devices. Ikbal et al. [26], Bali and Awasthi [27] and Misra et al. [28] have all done significant work on biofluid dynamics in the context of magnetic fields, while He [29,30] investigated the application of Homotopy perturbation method. A moving electrically conducting fluid will produce both electric and magnetic fields when exposed to a magnetic field. A body force called the Lorentz force is created when these fields interact, and it tends to oppose the liquid's movement [31]. When Sud et al. [32] investigated how a moving magnetic field affected blood flow, they found that a suitable moving magnetic field accelerated blood flow. Utilizing a long wavelength approximation technique and a fundamental mathematical model for blood flow in a uniformly branching channel with flexible walls. Agrawal and Anwaruddin [33] examined the influence of a magnetic field on blood flow. The research demonstrated that a magnetic field could serve as a blood pump in cardiac processes to improve blood circulation in arteries impacted by arterial abnormalities such as stenosis or arteriosclerosis.

The various uses of porous medium, such as fluid filtration, water flow across riverbeds, surface water and oil transportation, bile duct fluid mechanics, and blood circulation in small arteries, make their impact on fluid dynamics noteworthy. Researchers have been inspired by these real-world uses to study flow dynamics in various geometries that incorporate porous media [34]. The impact of magnetic forces on the fluid flow of a nanofluid through an inclined channel with permeable walls and different constrictions, located within a porous medium, was investigated by Prasad, K. M., and Yasa, P. R. [35]. Azmi, W. F. W. et al. [36] studied fractional Casson fluid flow in small arteries, highlighting the impact of slip conditions and cholesterol porosity on blood flow dynamics.

In the human body, arteries are rarely aligned horizontally or vertically. Many arteries, including the carotid, femoral, and coronary arteries, are naturally inclined as a result of anatomical form and posture. Modelling the artery as inclined allows us to include gravitational forces that influence blood flow and pressure distribution. According to studies, arterial inclination has a considerable impact on velocity profiles, wall shear stress, and pressure gradients, all of which are important in diagnosing vascular disorders like stenosis. Therefore, including an inclined configuration in cardiovascular models provides a more realistic and comprehensive knowledge of blood flow dynamics under various physiological conditions. Prasad, K.M. and Yasa, P.R. [37] investigated micropolar fluid behavior in an inclined permeable tube with a non-uniform cross-section with an explanation for non-newtonian fluid flow in tubes with multiple stenoses. Their results illustrate the importance of fluid dynamics in the development and potential treatment of cardiovascular diseases.

Many researchers describe the stenosis as mild and single or multiple, but arterial disease often involves a combination of stenotic and post-stenotic dilated segments. Sudha, T. et al. [38] analyzed the impact of stenosis and dilatation on arterial blood flow with suspended nanoparticles utilizing the Homotopy method. Maruthi Prasad, K. et al. [39] investigates the impact of stenosis and post-stenotic dilatation on Jeffrey fluid flow in arteries. Pincombe et al. [40] investigated the effects of post-stenotic enlargements in coronary arteries, emphasizing the need for a more comprehensive approach to modeling arterial disease. While considering the issue of post-stenotic dilations as an interesting mathematical problem with applications frequently in the vascular system, this article focuses on post-stenotic dilatations since they have more medicinal significance.

Motivated from the above investigations a mathematical model has been developed for fluid flow across an inclined stenosis and dilatation with the influence of a magnetic field through a porous medium. Blood has been described as a micropolar fluid flow that contains nanoparticles.

2. MATHEMATICAL MODEL

A Cylindrical polar coordinate system (r, θ, z) is considered, where the $Z-$axis coincides with the center line of the tube, and flow is assumed to be axisymmetric. Consider the flow of a micropolar fluid across an inclined stenosed artery with dilatation, characterized by fluid viscosity μ and density ρ.

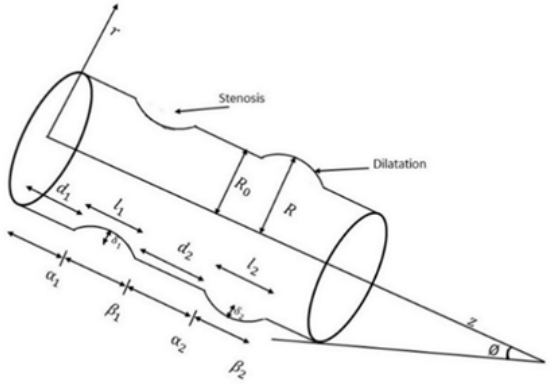

Figure 1. Geometry of the problem

The geometry of the problem, as shown in Figure 1, is given as

$$h(z) = \begin{cases} R_0 - \frac{\delta_i}{2}\left(1 + Cos\frac{2\pi}{l_i}\left(z - \alpha_i - \frac{l_i}{2}\right)\right), & for\ \alpha_i \le z \le \beta_i \\ R_0 & ; elsewhere \end{cases} \tag{1}$$

Where the maximum distance of the i[th] abnormal segment is denoted by δ_i, while R and R_0 signifies the radius of the affected artery and normal artery, respectively. The length of the i[th] abnormal segment is given by l_i, and the distance between the origin to the start of this segment is denoted by α_i as defined (Maruthi Prasad K. et al. [39] & Dhange M. et. al [41])

$$\alpha_i = \left(\sum_{j=1}^{i}(d_j + l_j)\right) - l_i \tag{2}$$

And β_i denotes the distance from the origin to the end of the i[th] abnormal segment and is given by

$$\beta_i = \left(\sum_{j=1}^{i}(d_j + l_j)\right) \tag{3}$$

The distance between the start of the i[th] abnormal section from the end of the (i-1)[th] segment is represent by d_i, for from the start of the segment if i =1

Accordingly, these are the governing equations for the fluid flow (Prasad, K. M. et al. [42])

$$\frac{\partial w_r}{\partial r} + \frac{w_r}{r} + \frac{\partial w_z}{\partial z} = 0 \tag{4}$$

$$R_e\delta\left(w_r\frac{\partial w_z}{\partial r} + w_z\frac{\partial w_z}{\partial z}\right) = -\frac{\partial p}{\partial z} + \frac{1}{N-1}\left(\frac{N}{r}\frac{\partial(rv_\theta)}{\partial r} + \frac{\partial^2 w_z}{\partial r^2} + \frac{1}{r}\frac{\partial w_z}{\partial r} + \delta^2\frac{\partial^2 w_z}{\partial z^2}\right) + (G_r\theta + B_r\sigma) + \frac{sin[\emptyset]}{F} - \frac{\mu\bar{w}}{K} + \bar{J}\times\bar{B} \tag{5}$$

$$R_e\delta^3\left(w_r\frac{\partial w_r}{\partial r} + w_z\cdot\frac{\partial w_r}{\partial z}\right) = -\frac{\partial p}{\partial r} + \frac{\delta^2}{N-1}\left(-N\frac{\partial v_\theta}{\partial z} + \frac{\partial^2 w_r}{\partial r^2} + \frac{1}{r}\frac{\partial w_r}{\partial r} - \frac{w_r}{r^2} + \delta^2\frac{\partial^2 w_z}{\partial z^2}\right) - \frac{cos[\emptyset]}{F} \tag{6}$$

$$\frac{jR_e\delta(1-N)}{N}\left(w_r\frac{\partial v_\theta}{\partial r} + w_z\frac{\partial v_\theta}{\partial z}\right) = -2v_\theta + \left(\delta^2\frac{\partial w_r}{\partial z} - \frac{\partial w_z}{\partial r}\right) + \frac{2-N}{m^2}\left(\frac{\partial}{\partial r}\left(\frac{1}{r}\frac{\partial(rv_\theta)}{\partial r}\right) + \delta^2\frac{\partial^2 v_\theta}{\partial z^2}\right) \tag{7}$$

$$\frac{R_e\delta\mu\overline{T_0}}{2\rho a^2}\left(w_r\frac{\partial\theta_t}{\partial r} + w_z\frac{\partial\theta_t}{\partial z}\right) = \frac{\overline{T_0}}{a^2}\left(\frac{1}{r}\frac{\partial}{\partial r}\left(r\frac{\partial\theta_t}{\partial r}\right)\right) + \frac{N_b\overline{T_0}}{a^2}\left(\frac{\partial\sigma}{\partial r}\right)\left(\frac{\partial\theta_t}{\partial r}\right) + \frac{N_t}{a^2}\left(\frac{\partial\theta_t}{\partial r}\right)^2 \tag{8}$$

$$\frac{4R_e\mu\overline{C_0}}{\rho a^2}\left(w_r\frac{\partial\sigma}{\partial r} + w_z\frac{\partial\sigma}{\partial z}\right) = \frac{(\rho c)_f}{(\rho c)_p}\frac{1}{a^2}\left[N_b\left(\frac{1}{r}\frac{\partial}{\partial r}\left(r\frac{\partial\sigma}{\partial r}\right)\right) + N_t\left(\frac{1}{r}\frac{\partial}{\partial r}\left(r\frac{\partial\theta_t}{\partial r}\right)\right)\right] \tag{9}$$

where $T = \frac{(\rho c)_f}{(\rho c)_p}$ is the ratio between the effective heat capacity of the nano particle material and heat capacity of the fluid. Here $F = \frac{1}{\rho g}$, $N = \frac{\mu}{\mu+K}$ is the coupling number $(0 \le N \le 1)$, $m = \frac{a^2K(2\mu+K)}{\gamma(\mu+K)}$ is the micro polar parameter. v_θ is the micro rotation in the θ direction.

In this context, ρ denotes fluid density, p represents fluid pressure, K indicates the permeability of the porous media, j micro gyration parameter, (μ) refers to viscosity, and F corresponds to body force. $\bar{J} \times \bar{B}$ represents the Lorentz force term in magnetohydrodynamics (where $\bar{J}$ denotes the current density vector and $\bar{B}$ signifies the magnetic field vector). Here, the microrotation vector and velocity are represented by $V = (0, v_\theta, 0)$ & $W = (w_r, 0, w_z)$ respectively
The non-dimensional variables are

$$\bar{\delta} = \frac{\delta}{R_0}, \bar{z} = \frac{z}{L}, \bar{r} = \frac{r}{R_0}, \overline{w_z} = \frac{w_z}{w_0}, \overline{w_r} = \frac{Lw_r}{w_0\delta}, \overline{w_\theta} = \frac{R_0\vartheta_\theta}{w_0}, \bar{J} = \frac{j}{R_0^2}, \bar{p} = \frac{P}{\frac{\mu w_0 L}{R_0^2}}, \bar{q} = \frac{q}{\pi R_0^2 w}, R_e = \frac{2\rho c_1 R_0}{\mu}, F = \frac{\mu U^h}{\rho g R_0^{h+1}},$$

$$N_b = \frac{(\rho c)_p D_{\bar{B}} \bar{C}_0}{(\rho c)_f}, N_t = \frac{(\rho c)_p D_T \bar{T}_0}{(\rho c)_f \beta}, G_r = \frac{g\beta \bar{T}_0 R_0^3}{\gamma^2}, B_r = \frac{g\beta \bar{C}_0 R_0^3}{\gamma^2}, \theta_t = \frac{T-\bar{T}_0}{\bar{T}_0}, \sigma = \frac{C-\bar{C}_0}{\bar{C}_0}, \bar{F} = \frac{F}{\mu W \lambda'}, M = \frac{\sigma R_0^2 B_0^2}{\rho\vartheta},$$

By using mild stenosis approximation, $\left(\frac{\delta}{R_0} \ll 1, Re * (2\delta/L0) \ll 1 \; and \; 2R_0/L_0(1)\right)$ and non-dimensional scheme to the equations (4) to (9), the equations become

$$\frac{\partial P}{\partial r} = -\frac{\cos\alpha}{F} \tag{10}$$

$$\frac{N}{r}\frac{\partial}{\partial r}(rV_\theta) + \frac{\partial^2 w}{\partial r^2} + \frac{1}{r}\frac{\partial w}{\partial r} + (1-N)\frac{\sin[\emptyset]}{F} + (1-N)(G_r\theta + B_r\sigma) - \frac{\mu w}{k} - Mw = (1-N)\frac{\partial P}{\partial z} \tag{11}$$

$$2V_\theta + \frac{\partial w}{\partial r} - \frac{2-N}{m^2}\frac{\partial}{\partial r}\left(\frac{1}{r}\frac{\partial}{\partial r}(rV_\theta)\right) = 0 \tag{12}$$

$$\frac{1}{r}\frac{\partial}{\partial r}\left(r\frac{\partial\theta}{\partial r}\right) + N_b\frac{\partial\sigma}{\partial r}\frac{\partial\theta}{\partial r} + N_t\left(\frac{\partial\theta}{\partial r}\right)^2 = 0 \tag{13}$$

$$\frac{1}{r}\frac{\partial}{\partial r}\left(r\frac{\partial\sigma}{\partial r}\right) + \frac{N_t}{N_b}\left(\frac{1}{r}\frac{\partial}{\partial r}\left(r\frac{\partial\theta}{\partial r}\right)\right) = 0 \tag{14}$$

The axial velocity, denoted by w, has a radius of R_0. The temperature profile, nanoparticle phenomena, local temperature, and local nanoparticle Grashof numbers, Brownian motion number, Thermophoresis parameter, micropolar parameter and coupling number are represented by $\theta, \sigma, B_r, G_r, N_b, \; N_t, m \; and \; N$. Additionally, $M = \sigma B_0^2$ is the magnetic parameter, μ is the viscosity, and k is the porous medium permeability.

The non-dimensional boundary conditions (Prasad, K. M., & Sudha, T. [43])

$$w = 0, V_\theta = 0, \theta = 0, \sigma = o \; at \; r = h(z) \tag{15}$$

$$\frac{\partial w}{\partial r} = 0, \frac{\partial\theta}{\partial r} = 0, \frac{\partial\sigma}{\partial r} = 0 \; at \; r = 0 \tag{16}$$

$$V_\theta \text{ is finite at } r = h(z) \tag{17}$$

3. METHOD OF SOLUTION

The coupled equations are solved using the Homotopy Perturbation Method (HPM). The Homotopy perturbation method (HPM) has been used to determine the solutions of the coupled equations (13) and (14).

$$H(q,\theta) = (1-q)[L(\theta) - L(\theta_{10})] + q\left[L(\theta) + N_b\frac{\partial\sigma}{\partial r}\cdot\frac{\partial\theta}{\partial r} + N_t\left(\frac{\partial\theta}{\partial r}\right)^2\right] \tag{18}$$

$$H(q,\theta) = L(\theta) - L(\theta_{10}) + qL(\theta_{10}) + q\left[N_b\frac{\partial\sigma}{\partial r}\cdot\frac{\partial\theta}{\partial r} + N_t\left(\frac{\partial\theta}{\partial r}\right)^2\right] \tag{19}$$

$$H(q,\sigma) = (1-q)[L(\sigma) - L(\sigma_{10})] + q\left[L(\sigma) + \frac{N_t}{N_b}\left(\frac{1}{r}\frac{\partial}{\partial r}\left(r\frac{\partial\theta}{\partial r}\right)\right)\right] \tag{20}$$

$$H(q,\sigma) = L(\sigma) - L(\sigma_{10}) + qL(\sigma_{10}) + q\left[\frac{N_t}{N_b}\left(\frac{1}{r}\frac{\partial}{\partial r}\left(r\frac{\partial\theta}{\partial r}\right)\right)\right] \tag{21}$$

Where, q is the embedding parameter $(0 \le q \le 1)$, $L \equiv \frac{1}{r}\frac{\partial}{\partial r}\left(r\cdot\frac{\partial}{\partial r}\right)$ is a linear operator, $\theta_0 \; ahd \; \sigma_0$ are the initial guesses, given by

$$\theta_0(r,z) = \left(\frac{r^2-h^2}{4}\right), \quad \sigma_0(r,z) = -\left(\frac{r^2-h^2}{4}\right) \tag{22}$$

Define

$$\theta(r,z) = \theta_0 + q\theta_1 + q^2\theta_2 + \cdots \tag{23}$$

$$\sigma(r,z) = \sigma_0 + q\sigma_1 + q^2\sigma_2 + \cdots \tag{24}$$

The Convergence of equations (23) and (24) is depending up on the non – linear component of the expression. Utilizing the same procedure as applied by (30), the solutions for temperature profile (θ) and nanoparticle phenomenon (σ) for q = 1 are

$$\theta(r,z) = \frac{1}{64}(N_b - N_t)(r^2 - h^2) - \left(\frac{1}{18}N_b(r^3 - h^3) + \frac{N_t}{36864}(N_b^2 + N_t^2)(r^4 - h^4)(r^6 - h^6)\right) \tag{25}$$

$$\sigma(r,z) = \frac{-1}{4}(r^2 - h^2)\frac{N_t}{N_b} + \frac{Nt}{N_b}\left(\frac{1}{18}N_b(r^3 - h^3) + \frac{1}{36864}(N_b^2 + N_t^2)(r^6 - h^6)\right). \tag{26}$$

Substituting equations (25) and (26) in (11) and using boundary conditions

$$\frac{\partial w}{\partial r} = -NV_\theta + (1-N)\frac{r}{2}\frac{dP}{dz} - (1-N)\frac{r}{2}\frac{sin[\emptyset]}{F} - (1-N)\left[G_r\left(\frac{1}{64}(N_b - N_t)\left(\frac{r^3}{4} - \frac{h^2 r}{2}\right) - \left(\frac{1}{18}N_b\left(\frac{r^4}{5} - \frac{h^3 r}{2}\right) + \frac{N_t(N_t^2+N_b^2)}{36864}\left(\frac{r^{11}}{12} - \frac{r^5 h^6}{6} - \frac{r^7 h^4}{8} + \frac{r h^{10}}{2}\right)\right)\right) + B_r\left(\frac{-1}{4}\left(\frac{r^3}{4} - \frac{h^2 r}{2}\right)\frac{N_t}{N_b} + \frac{N_t}{N_b}\left(\frac{N_b}{18}\left(\frac{r^4}{5} - \frac{h^3 r^2}{2}\right) + \frac{(N_b^2+N_t^2)}{3686u}\left(\frac{r^7}{8} - \frac{h^6 r}{2}\right)\right)\right)\right] + \left(\frac{\mu}{k} + M\right)\frac{wr}{2} \tag{27}$$

Substitute (27) and (12), we get the expression for V_θ

$$V_\theta = C_2(z)I_1(mr) + C_3(z)K_1(mr) - \frac{(1-N)r}{2(2-N)}\left(\frac{dP}{dz} - \frac{\sin[\emptyset]}{F}\right) + \left(\frac{1-N}{2-N}\right)\left[G_r(N_b - N_t)\left(\frac{r}{32m^2} - \frac{h^2 r}{128} + \frac{r^3}{256}\right) - G_r N_b\left(\frac{1}{2m^4} - \frac{rh^3}{36} + \frac{r^2}{6m^2} + \frac{r^4}{90}\right) - \frac{G_r N_t(N_b^2+N_t^2)}{36864}\left(\frac{7372800r}{m'^0} - \frac{1152h^4 r}{m^6} - \frac{32h^6 r}{m^4} + \frac{h^{10}r}{2} + \frac{921600r^3}{m^8} - \frac{144h^4 r^3}{m^4} - \frac{4h^6 r^3}{m^2} + \frac{38400r^5}{m^6} - \frac{6h^4 r^5}{m^2} - \frac{h^6 r^5}{6} + \frac{800r^7}{m^4} - \frac{h^4 r^7}{8} + \frac{10r^9}{m^2} + \frac{r^{11}}{12}\right) - \frac{B_r N_t}{N_b}\left(\frac{r}{2m^2} - \frac{rh^2}{8} + \frac{r^3}{16}\right) + B_r N_t\left(\frac{1}{2m^4} - \frac{rh^3}{36} + \frac{r^2}{6m^2} + \frac{r^4}{90}\right) + \frac{B_r(N_b^2+N_t^2)}{36864}\left(\frac{N_t}{N_b}\right)\left(\frac{1152^r}{m^6} - \frac{h^6 r}{2} + \frac{144r^3}{m^4} + \frac{6r^5}{m^2} + \frac{r^7}{8}\right) - \frac{wr}{2(2-N)}\left(\frac{\mu}{k} + M\right)\right] \tag{28}$$

where, $I_1(mr)$ and $K_1(mr)$ the 1st and 2nd order modified Bessel functions, respectively.
Substitute equation (28) into equation (27), and by applying the boundary conditions (15-17), the velocity is

$$w[z,r] = \frac{1}{\left[1-\left(\frac{\mu}{k}+M\right)\frac{r^2}{2(2-N)}\right]}\left[-NC_2(z)\frac{I_0(mr)}{m} + \frac{(1-N)}{(2-N)}\frac{r^2}{2}\left(\frac{dP}{dz} - \frac{\sin[\emptyset]}{F}\right) - \frac{(1-N)}{(2-N)}\left(G_r(N_b - N_t)\left(\frac{Nr^2}{64m^2} + \frac{r^4}{512} - \frac{r^2h^2}{128}\right) - G_r N_b\left(\frac{Nr}{2m^4} + \frac{Nr^3}{18m^2} + \frac{r^5}{225} - \frac{r^2h^2}{36}\right) - \frac{G_r N_t(N_b^2+N_t^2)}{36864}\left(\frac{7372800Nr^2}{2m^{10}} + \frac{230400Nr^4}{m^8} - \frac{576Nr^2h^2}{m^6} + \frac{6400Nr^6}{m^6} - \frac{16h^6Nr^2}{m^4} - \frac{36h^4r^4}{m^4} + \frac{100Nr^8}{m^4} - \frac{Nh^6r^4}{m^2} + \frac{Nr^{10}}{m^2} - \frac{Nh^4r^6}{m^2} + \frac{r^{12}}{72} - \frac{r^6h^6}{18} - \frac{r^8h^4}{32} + \frac{r^2h^{10}}{2}\right) - \frac{B_r N_t}{N_b}\left(\frac{Nr^2}{4m^2} + \frac{r^4}{32} - \frac{r^2h^2}{8}\right) + B_r N_t\left(\frac{Nr}{2m^4} + \frac{Nr^3}{18m^2} + \frac{r^5}{225} - \frac{r^2h^3}{36}\right) + \frac{B_r(N_t^2+N_b^2)}{36864}\frac{Nt}{Nb}\left(\frac{576Nr^2}{m^6} + \frac{36Nr^4}{m^4} + \frac{Nr^6}{m^2} - \frac{r^8}{32} - \frac{h^6r^2}{2}\right)\right) + C_4\right] \tag{29}$$

where,

$$C_4 = NC_2\frac{I_0(mh)}{m} - \frac{(1-N)}{(2-N)}\frac{h^2}{q}\left(\frac{dP}{dz} - \frac{\sin[\emptyset]}{F}\right) + \frac{(1-N)}{(2-N)}\left(G_r(N_b - N_t)\left(\frac{Nh^2}{64m^2} - \frac{3h^4}{512}\right) - G_r N_b\left(\frac{Nh}{2m^4} + \frac{Nh^3}{18m^2} - \frac{7h^5}{300}\right) - \frac{G_r N_t(N_b^2+N_t^2)}{36864}\left(\frac{3686400Nh^2}{m^{10}} + \frac{230400Nh^4}{m^{10}} + \frac{5824Nh^6}{m^6} + \frac{48Nh^8}{m^4} - \frac{Nh'^0}{m^2} + \frac{41h^{12}}{96}\right) - \frac{B_r N_t}{Nb}\left(\frac{Nh^2}{4m^2} - \frac{3h^4}{8}\right) + B_r N_t\left(\frac{Nh}{2m^4} + \frac{Nh^3}{18m^2} - \frac{7h^5}{300}\right) + \frac{B_r(N_t^2+N_b^2)}{36864}\frac{Nt}{Nb}\left(\frac{576Nh^2}{m^6} + \frac{36Nh^4}{m^4} + \frac{Nh^6}{m^2} - \frac{15h^8}{32}\right)\right)$$

$$C_2 = \frac{1}{I_1(mh)}\left[\frac{(1-N)}{(2-N)}\left(\frac{dP}{dz} - \frac{\sin[\emptyset]}{F}\right)\frac{h}{2} - \frac{(1-N)}{(2-N)}\left(G_r(N_b - N_t)\left(\frac{h}{2m^2} - \frac{h^3}{256}\right) - G_r N_b\left(\frac{1}{2m^4} + \frac{h^2}{6m^2} - \frac{h^4}{60}\right) - \frac{G_r N_b(N_b^2+N_t^2)}{36864}\left(\frac{7372800h}{m^{10}} + \frac{921600h^3}{m^8} + \frac{37248h^5}{m^6} + \frac{624h^7}{m^4} + \frac{7h^{11}}{24}\right) - \frac{B_r N_t}{N_b}\left(\frac{h}{2m^2} - \frac{h^3}{16}\right) + B_r N_t\left(\frac{1}{2m^4} + \frac{h^2}{6m^2} - \frac{h^4}{60}\right) + \frac{B_r(N_b^2+N_t^\nu)}{36864}\frac{N_t}{N_b}\left(\frac{1152h}{m^6} + \frac{144h^3}{m^4} + \frac{6h^5}{m^2} - \frac{3h^7}{8}\right)\right)\right]$$

Dimension less flux (Q) can be determined as follows:

$$Q = \int_0^h 2rw\, dr \tag{30}$$

$$Q = \left[\left(\frac{Nh^2}{m}\frac{I_0(mh)}{I_1(mh)} - \frac{2Nh}{m}\right) + \frac{\left(\frac{\mu}{k}+M\right)}{(2-N)}\left(\frac{N}{m}\frac{I_0(mh)}{I_1(mh)}\frac{h^4}{4} - \frac{Nh^3}{m} + \frac{2Nh^2}{m}\frac{I_2(mh)}{I_1(mh)}\right)\left(\frac{(1-N)}{(2-N)}\left(\frac{dP}{dz} - \frac{\sin[\emptyset]}{F}\right)\frac{h}{2} - \right.\right.$$
$$\frac{(1-N)}{(2-N)}\left(G_r(N_b - N_t)\left(\frac{h}{32m^2} - \frac{h^3}{256}\right) - G_rN_b\left(\frac{1}{2m^4} + \frac{h^2}{6m^2} - \frac{h^4}{60}\right) - \frac{G_rN_t\left(N_b^2+N_t^2\right)}{36864}\left(\frac{7372800h}{m^{10}} + \frac{37248h^5}{m^6} + \frac{6244^7}{m^4} + \right.\right.$$
$$\left.\left.\frac{7h^{11}}{24} + \frac{921600h^3}{m^8}\right) - \frac{B_rN_t}{N_b}\left(\frac{h}{2m^2} - \frac{h^3}{16}\right) + B_rN_t\left(\frac{1}{2m^4} + \frac{h^2}{6m^2} - \frac{h^4}{60}\right) + \frac{B_r\left(N_b^2+N_t^2\right)}{36864}\left(\frac{N_t}{N_b}\right)\left(\frac{1152h}{m^6} + \frac{144h^3}{m^4} + \frac{6h^5}{m^2} - \right.\right.$$
$$\left.\left.\left.\left.\frac{3h^7}{8}\right)\right)\right)\right] + \frac{(1-N)}{(2-N)}\left(\frac{-h^4}{4} - \frac{h^6}{24}\frac{\left(\frac{\mu}{k}+M\right)}{(2-N)}\right)\left(\frac{dP}{dz} - \frac{\sin\alpha}{F}\right) - \frac{(1-N)}{(2-N)}\left[G_r(N_b - N_t)\left(\left(\frac{-Nh^4}{128m^2} + \frac{379h^6}{1536}\right) + \right.\right.$$
$$\left.\left(\frac{-Nh^6}{768m^2} + \frac{755h^6}{12288}\right)\frac{\left(\frac{\mu}{k}+M\right)}{(2-N)}\right) - G_rN_b\left(\left(-\frac{Nh^3}{6m^4} - \frac{Nh^5}{30m^2} + \frac{3h^7}{280}\right) + \left(\frac{-Nh^5}{40m^4} - \frac{Nh^7}{168m^2} + \frac{11h^9}{6480}\right)\frac{\left(\frac{\mu}{k}+M\right)}{(2-N)}\right) -$$
$$\frac{G_rN_t\left(N_t^2+N_b^2\right)}{36864}\left(\left(\frac{-1843200Nh^4}{m^{10}} - \frac{153600Nh^6}{m^8} - \frac{2255Nh^8}{m^6} - \frac{24Nh^{10}}{m^4} + \frac{7Nh^{12}}{24m^2} - \frac{73h^{14}}{210}\right) + \left(\frac{-307200Nh^6}{m^{10}} - \frac{28800Nh^8}{m^8} - \right.\right.$$
$$\left.\left.\frac{912Nh^6}{m^6} - \frac{65Nh^{12}}{6m^4} + \frac{27Nh^{14}}{280m^2} - \frac{59h^{16}}{1920}\right)\frac{\left(\frac{\mu}{k}+m\right)}{(2-N)}\right) - \frac{B_rNt}{N_b}\left(\left(\frac{-Nh^4}{8m^2} + \frac{31h^4}{192}\right) + \left(\frac{-Nh^6}{48m^2} + \frac{59h^8}{768}\right)\frac{\left(\frac{\mu}{k}+M\right)}{(2-N)}\right) +$$
$$B_rN_t\left(\left(-\frac{Nh^3}{6m^4} - \frac{Nh^5}{30m^2} + \frac{3h^7}{280}\right) + \left(\frac{-Nh^5}{40m^4} - \frac{Nh^7}{168m^2} + \frac{11h^9}{6480}\right)\frac{\left(\frac{\mu}{k}+M\right)}{(2-N)}\right) + \frac{B_r\left(N_t^2+N_b^2\right)}{36864}\left(\frac{N_t}{N_b}\right)\left(\left(\frac{-288Nh^4}{m^6} - \frac{24Nh^6}{m^4} - \right.\right.$$
$$\left.\left.\left.\frac{3Nh^8}{4m^2} + \frac{19h^{10}}{80}\right) + \left(\frac{-48Nh^6}{m^6} - \frac{9Nh^8}{2m^4} - \frac{3Nh^{10}}{20m^2} + \frac{h^{12}}{32}\right)\frac{\left(\frac{\mu}{k}+M\right)}{(2-N)}\right)\right] \tag{31}$$

From equation (31), $\frac{dP}{dz}$ is

$$\frac{dP}{dz} = \frac{\mathrm{Sin}[\emptyset]}{F} + \left[\frac{1}{\left(\left(\frac{\mathrm{Nh}^3 I_0(mh)}{2m\, I_1(mh)} - \frac{\mathrm{Nh}^2}{m} - \frac{\mathrm{h}^4}{4}\right) + \left(\frac{\mathrm{N}}{m} * \frac{I_0(mh)\mathrm{h}^5}{I_1(mh)\,8} - \frac{\mathrm{Nh}^4}{2m} - \frac{\mathrm{Nh}^3}{m} * \frac{I_2(mh)}{I_1(mh)} - \frac{\mathrm{h}^6}{24}\right)\left(\frac{\frac{\mu}{k}+M}{(2-\mathrm{N})}\right)\right)}\right]\left(\frac{Q(2-\mathrm{N})}{(1-\mathrm{N})} + \right.$$
$$\left(\left(\frac{\mathrm{Nh}^2}{2m} * \frac{I_0(mh)}{I_1(mh)} - \frac{2\mathrm{Nh}}{m}\right) + \left(\frac{\mathrm{N}}{m} * \frac{I_0(mh)}{I_1(mh)}\frac{\mathrm{h}^4}{4} - \frac{\mathrm{Nh}^3}{m} - \frac{2\mathrm{Nh}^2}{m}\frac{I_2(mh)}{I_1(mh)}\right)\left(\frac{\left(\frac{\mu}{k}+M\right)}{(2-\mathrm{N})}\right)\right)\left(G_r(N_b - N_t)\left(\frac{h}{32m^2} - \frac{h^3}{256}\right) - \right.$$
$$G_rN_b\left(\frac{1}{2m^4} + \frac{h^2}{6m^2} - \frac{h^4}{60}\right) - \frac{G_rN_t\left(N_b^2+N_t^2\right)}{36864}\left(\frac{7372800h}{m^{10}} + \frac{37248h^5}{m^6} + \frac{6244^7}{m^4} + \frac{7h^{11}}{24} + \frac{921600h^3}{m^8}\right) -$$
$$\frac{B_rN_t}{N_b}\left(\frac{h}{2m^2} - \frac{h^3}{16}\right) + B_rN_t\left(\frac{1}{2m^4} + \frac{h^2}{6m^2} - \frac{h^4}{60}\right) + \frac{B_r\left(N_b^2+N_t^2\right)}{36864}\left(\frac{N_t}{N_b}\right)\left(\frac{1152h}{m^6} + \frac{144h^3}{m^4} + \frac{6h^5}{m^2} - \frac{3h^7}{8}\right) +$$
$$\left(G_r(N_b - N_t)\left(\left(\frac{-Nh^4}{128m^2} + \frac{379h^6}{1536}\right) + \left(\frac{-Nh^6}{768m^2} + \frac{755h^6}{12288}\right)\frac{\left(\frac{\mu}{k}+M\right)}{(2-N)}\right) - G_rN_b\left(\left(-\frac{Nh^3}{6m^4} - \frac{Nh^5}{30m^2} + \frac{3h^7}{280}\right) + \right.$$
$$\left(\frac{-Nh^5}{40m^4} - \frac{Nh^7}{168m^2} + \frac{11h^9}{6480}\right)\frac{\left(\frac{\mu}{k}+M\right)}{(2-N)}\right) - \frac{G_rN_t\left(N_t^2+N_b^2\right)}{36864}\left(\left(\frac{-1843200Nh^4}{m^{10}} - \frac{153600Nh^6}{m^8} - \frac{2255Nh^8}{m^6} - \frac{24Nh^{10}}{m^4} + \frac{7Nh^{12}}{24m^2} - \right.\right.$$
$$\left.\left.\frac{73h^{14}}{210}\right) + \left(\frac{-307200Nh^6}{m^{10}} - \frac{28800Nh^8}{m^8} - \frac{912Nh^6}{m^6} - \frac{65Nh^{12}}{6m^4} + \frac{27Nh^{14}}{280m^2} - \frac{59h^{16}}{1920}\right)\frac{\left(\frac{\mu}{k}+m\right)}{(2-N)}\right) - \frac{B_rNt}{N_b}\left(\left(\frac{-Nh^4}{8m^2} + \frac{31h^4}{192}\right) + \right.$$
$$\left(\frac{-Nh^6}{48m^2} + \frac{59h^8}{768}\right)\frac{\left(\frac{\mu}{k}+M\right)}{(2-N)}\right) + B_rN_t\left(\left(-\frac{Nh^3}{6m^4} - \frac{Nh^5}{30m^2} + \frac{3h^7}{280}\right) + \left(\frac{-Nh^5}{40m^4} - \frac{Nh^7}{168m^2} + \frac{11h^9}{6480}\right)\frac{\left(\frac{\mu}{k}+M\right)}{(2-N)}\right) +$$
$$\left.\left.\frac{B_r\left(N_t^2+N_b^2\right)}{36864}\left(\frac{N_t}{N_b}\right)\left(\left(\frac{-288Nh^4}{m^6} - \frac{24Nh^6}{m^4} - \frac{3Nh^8}{4m^2} + \frac{19h^{10}}{80}\right) + \left(\frac{-48Nh^6}{m^6} - \frac{9Nh^8}{2m^4} - \frac{3Nh^{10}}{20m^2} + \frac{h^{12}}{32}\right)\frac{\left(\frac{\mu}{k}+M\right)}{(2-N)}\right)\right)\right) \tag{32}$$

The pressure drop per wave length $\Delta p = p(0) - p(\lambda)$ is

$$\Delta p = -\int_0^1 \frac{dP}{dz}\, dz$$

$$\Delta p = -\int_0^1 \left[\frac{Sin[\emptyset]}{F} + \left[\frac{1}{\left(\left(\frac{Nh^3 I_0(mh)}{2m\, I_1(mh)} - \frac{Nh^2}{m} - \frac{h^4}{4} \right) + \left(\frac{N}{m} * \frac{I_0(mh) h^5}{I_1(mh)\ 8} - \frac{Nh^4}{2m} - \frac{Nh^3}{m} * \frac{I_2(mh)}{I_1(mh)} - \frac{h^6}{24} \right) \left(\frac{\frac{\mu}{\kappa}+M}{(2-N)} \right) \right)} \right] \left(\frac{Q(2-N)}{(1-N)} + \left(\left(\frac{Nh^2}{2m} * \frac{I_0(mh)}{I_1(mh)} - \frac{2Nh}{m} \right) + \left(\frac{N}{m} * \frac{I_0(mh)}{I_1(mh)} \frac{h^4}{4} - \frac{Nh^3}{m} - \frac{2Nh^2}{m} \frac{I_2(mh)}{I_1(mh)} \right) \left(\frac{\left(\frac{\mu}{\kappa}+M\right)}{(2-N)} \right) \right) \left(G_r(N_b - N_t) \left(\frac{h}{32m^2} - \frac{h^3}{256} \right) - G_r N_b \left(\frac{1}{2m^4} + \frac{h^2}{6m^2} - \frac{h^4}{60} \right) - \frac{G_r N_t (N_b^2 + N_t^2)}{36864} \left(\frac{7372800h}{m^{10}} + \frac{37248h^5}{m^6} + \frac{624h^7}{m^4} + \frac{7h^{11}}{24} + \frac{921600h^3}{m^8} \right) - \frac{B_r N_t}{N_b} \left(\frac{h}{2m^2} - \frac{h^3}{16} \right) + B_r N_t \left(\frac{1}{2m^4} + \frac{h^2}{6m^2} - \frac{h^4}{60} \right) + \frac{B_r (N_b^2 + N_t^2)}{36864} \left(\frac{N_t}{N_b} \right) \left(\frac{1152h}{m^6} + \frac{144h^3}{m^4} + \frac{6h^5}{m^2} - \frac{3h^7}{8} \right) \right) + \left(G_r(N_b - N_t) \left(\left(\frac{-Nh^4}{128m^2} + \frac{379h^6}{1536} \right) + \left(\frac{-Nh^6}{768m^2} + \frac{755h^6}{12288} \right) \frac{\left(\frac{\mu}{k}+M\right)}{(2-N)} \right) - G_r N_b \left(\left(-\frac{Nh^3}{6m^4} - \frac{Nh^5}{30m^2} + \frac{3h^7}{280} \right) + \left(\frac{-Nh^5}{40m^4} - \frac{Nh^7}{168m^2} + \frac{11h^9}{6480} \right) \frac{\left(\frac{\mu}{k}+M\right)}{(2-N)} \right) - \frac{G_r N_t (N_t^2 + N_b^2)}{36864} \left(\left(\frac{-1843200Nh^4}{m^{10}} - \frac{153600Nh^6}{m^8} - \frac{2255Nh^8}{m^6} - \frac{24Nh^{10}}{m^4} + \frac{7Nh^{12}}{24m^2} - \frac{73h^{14}}{210} \right) + \left(\frac{-307200Nh^6}{m^{10}} - \frac{28800Nh^8}{m^8} - \frac{912Nh^6}{m^6} - \frac{65Nh^{12}}{6m^4} + \frac{27Nh^{14}}{280m^2} - \frac{59h^{16}}{1920} \right) \frac{\left(\frac{\mu}{k}+m\right)}{(2-N)} \right) - \frac{B_r Nt}{N_b} \left(\left(\frac{-Nh^4}{8m^2} + \frac{31h^4}{192} \right) + \left(\frac{-Nh^6}{48m^2} + \frac{59h^8}{768} \right) \frac{\left(\frac{\mu}{k}+M\right)}{(2-N)} \right) + B_r N_t \left(\left(-\frac{Nh^3}{6m^4} - \frac{Nh^5}{30m^2} + \frac{3h^7}{280} \right) + \left(\frac{-Nh^5}{40m^4} - \frac{Nh^7}{168m^2} + \frac{11h^9}{6480} \right) \frac{\left(\frac{\mu}{k}+M\right)}{(2-N)} \right) + \frac{B_r (N_t^2 + N_b^2)}{36864} \left(\frac{N_t}{N_b} \right) \left(\left(\frac{-288Nh^4}{m^6} - \frac{24Nh^6}{m^4} - \frac{3Nh^8}{4m^2} + \frac{19h^{10}}{80} \right) + \left(\frac{-48Nh^6}{m^6} - \frac{9Nh^8}{2m^4} - \frac{3Nh^{10}}{20m^2} + \frac{h^{12}}{32} \right) \frac{\left(\frac{\mu}{k}+M\right)}{(2-N)} \right) \right) \right) \right] dz \quad (33)$$

Also, flow resistance λ is defined as

$$\lambda = \frac{\Delta p}{Q}$$

$$\lambda = \frac{-1}{Q} \int_0^1 \left[\frac{Sin[\emptyset]}{F} + \left[\frac{1}{\left(\left(\frac{Nh^3 I_0(mh)}{2m\, I_1(mh)} - \frac{Nh^2}{m} - \frac{h^4}{4} \right) + \left(\frac{N}{m} * \frac{I_0(mh) h^5}{I_1(mh)\ 8} - \frac{Nh^4}{2m} - \frac{Nh^3}{m} * \frac{I_2(mh)}{I_1(mh)} - \frac{h^6}{24} \right) \left(\frac{\frac{\mu}{\kappa}+M}{(2-N)} \right) \right)} \right] \left(\frac{Q(2-N)}{(1-N)} + \left(\left(\frac{Nh^2}{2m} * \frac{I_0(mh)}{I_1(mh)} - \frac{2Nh}{m} \right) + \left(\frac{N}{m} * \frac{I_0(mh)}{I_1(mh)} \frac{h^4}{4} - \frac{Nh^3}{m} - \frac{2Nh^2}{m} \frac{I_2(mh)}{I_1(mh)} \right) \left(\frac{\left(\frac{\mu}{\kappa}+M\right)}{(2-N)} \right) \right) \left(G_r(N_b - N_t) \left(\frac{h}{32m^2} - \frac{h^3}{256} \right) - G_r N_b \left(\frac{1}{2m^4} + \frac{h^2}{6m^2} - \frac{h^4}{60} \right) - \frac{G_r N_t (N_b^2 + N_t^2)}{36864} \left(\frac{7372800h}{m^{10}} + \frac{37248h^5}{m^6} + \frac{624h^7}{m^4} + \frac{7h^{11}}{24} + \frac{921600h^3}{m^8} \right) - \frac{B_r N_t}{N_b} \left(\frac{h}{2m^2} - \frac{h^3}{16} \right) + B_r N_t \left(\frac{1}{2m^4} + \frac{h^2}{6m^2} - \frac{h^4}{60} \right) + \frac{B_r (N_b^2 + N_t^2)}{36864} \left(\frac{N_t}{N_b} \right) \left(\frac{1152h}{m^6} + \frac{144h^3}{m^4} + \frac{6h^5}{m^2} - \frac{3h^7}{8} \right) \right) + \left(G_r(N_b - N_t) \left(\left(\frac{-Nh^4}{128m^2} + \frac{379h^6}{1536} \right) + \left(\frac{-Nh^6}{768m^2} + \frac{755h^6}{12288} \right) \frac{\left(\frac{\mu}{k}+M\right)}{(2-N)} \right) - G_r N_b \left(\left(-\frac{Nh^3}{6m^4} - \frac{Nh^5}{30m^2} + \frac{3h^7}{280} \right) + \left(\frac{-Nh^5}{40m^4} - \frac{Nh^7}{168m^2} + \frac{11h^9}{6480} \right) \frac{\left(\frac{\mu}{k}+M\right)}{(2-N)} \right) - \frac{G_r N_t (N_t^2 + N_b^2)}{36864} \left(\left(\frac{-1843200Nh^4}{m^{10}} - \frac{153600Nh^6}{m^8} - \frac{2255Nh^8}{m^6} - \frac{24Nh^{10}}{m^4} + \frac{7Nh^{12}}{24m^2} - \frac{73h^{14}}{210} \right) + \left(\frac{-307200Nh^6}{m^{10}} - \frac{28800Nh^8}{m^8} - \frac{912Nh^6}{m^6} - \frac{65Nh^{12}}{6m^4} + \frac{27Nh^{14}}{280m^2} - \frac{59h^{16}}{1920} \right) \frac{\left(\frac{\mu}{k}+m\right)}{(2-N)} \right) - \frac{B_r Nt}{N_b} \left(\left(\frac{-Nh^4}{8m^2} + \frac{31h^4}{192} \right) + \left(\frac{-Nh^6}{48m^2} + \frac{59h^8}{768} \right) \frac{\left(\frac{\mu}{k}+M\right)}{(2-N)} \right) + B_r N_t \left(\left(-\frac{Nh^3}{6m^4} - \frac{Nh^5}{30m^2} + \frac{3h^7}{280} \right) + \left(\frac{-Nh^5}{40m^4} - \frac{Nh^7}{168m^2} + \frac{11h^9}{6480} \right) \frac{\left(\frac{\mu}{k}+M\right)}{(2-N)} \right) + \frac{B_r (N_t^2 + N_b^2)}{36864} \left(\frac{N_t}{N_b} \right) \left(\left(\frac{-288Nh^4}{m^6} - \frac{24Nh^6}{m^4} - \frac{3Nh^8}{4m^2} + \frac{19h^{10}}{80} \right) + \left(\frac{-48Nh^6}{m^6} - \frac{9Nh^8}{2m^4} - \frac{3Nh^{10}}{20m^2} + \frac{h^{12}}{32} \right) \frac{\left(\frac{\mu}{k}+M\right)}{(2-N)} \right) \right) \right) \right] dz \quad (34)$$

Equation Δp is used to calculate the pressure drop when there is no stenosis h = 1, which is indicated by Δp_n. The normal artery's flow resistance is represented by

$$\lambda_n = \frac{\Delta p_n}{q} \tag{35}$$

The Normalized flow resistance denoted by

$$\bar{\lambda} = \frac{\lambda}{\lambda_n} \tag{36}$$

Dimensionless shear stresses can be determined as follows

$$\tau_{rz} = \frac{1}{(1-N)}\frac{\partial w}{\partial r} + \frac{N}{(1-N)}V_\theta \tag{37}$$

$$\tau_{zr} = \frac{\partial w}{\partial r} - \frac{1}{(1-N)}V_\theta \tag{38}$$

$$\tau_{rz} = \frac{r}{2}\left(\frac{dp}{dz} - \frac{\sin\emptyset}{F}\right) - \left[G_r\left(\frac{1}{64}(N_b - N_t)\left(\frac{r^3}{4} - \frac{h^2 r}{2}\right) - \left(\frac{1}{18}N_b\left(\frac{r^4}{5} - \frac{h^3 r}{2}\right) + \frac{N_t(N_t^2+N_b^2)}{36864}\left(\frac{r^{11}}{12} - \frac{r^5 h^6}{6} - \frac{r^7 h^4}{8} + \frac{r h^{10}}{2}\right)\right)\right) + B_r\left(\frac{-1}{4}\left(\frac{r^3}{4} - \frac{h^2 r}{2}\right)\frac{N_t}{N_b} + \frac{N_t}{N_b}\left(\frac{N_b}{18}\left(\frac{r^4}{5} - \frac{h^3 r^2}{2}\right) + \frac{(N_b^2+N_t^2)}{36864}\left(\frac{r^7}{8} - \frac{h^6 r}{2}\right)\right)\right)\right] + \left(\frac{\mu}{k} + M\right)\frac{wr}{2(1-N)} \tag{39}$$

$$\tau_{zr} = \frac{-N(2-N)r}{(1-N)}C_2(z)I_1(mr) + \frac{r}{2}\left(\frac{dP}{dz} - \frac{\sin\emptyset}{F}\right) - G_r(N_b - N_t)\left(\frac{Nr}{32m^2} - \frac{h^2 r}{128} + \frac{r^3}{256}\right) + G_r N_b\left(\frac{N}{2m^4} - \frac{rh^3}{36} + \frac{Nr^2}{6m^2} + \frac{r^4}{90}\right) + \frac{G_r N_t(N_b^2+N_t^2)}{36864}\left(\frac{7372800Nr}{m^{10}} - \frac{1152Nh^4 r}{m^6} - \frac{32Nh^6 r}{m^4} + \frac{921600r^3}{m^8} - \frac{144Nh^4 r^3}{m^4} - \frac{4Nh^6 r^3}{m^2} + \frac{38400Nr^5}{m^6} - \frac{6Nh^4 r^5}{m^2} + \frac{800Nr^7}{m^4} + \frac{10Nr^9}{m^2} - \frac{h^4 r^7}{8} - \frac{h^6 r^5}{6} + \frac{h^{10} r}{2} + \frac{r^{11}}{12}\right) + \frac{B_r N_t}{N_b}\left(\frac{Nr}{2m^2} - \frac{rh^2}{8} + \frac{r^3}{16}\right) - B_r N_t\left(\frac{N}{2m^4} - \frac{rh^3}{36} + \frac{Nr^2}{6m^2} + \frac{r^4}{90}\right) - \frac{B_r(N_b^2+N_t^2)}{36864}\left(\frac{N_t}{N_b}\right)\left(\frac{1152Nr}{m^6} + \frac{144Nr^3}{m^4} + \frac{6Nr^5}{m^2} - \frac{h^6 r}{2} + \frac{r^7}{8}\right) + \frac{wr}{2(1-N)}\left(\frac{\mu}{k} + M\right) \tag{40}$$

where

$$C_2 = \frac{1}{I_1(mh)}\left[\frac{(1-N)}{(2-N)}\left(\frac{dP}{dz} - \frac{\sin\emptyset}{F}\right)\frac{h}{2} - \frac{(1-N)}{(2-N)}\left(G_r(N_b - N_t)\left(\frac{h}{2m^2} - \frac{h^3}{256}\right) - G_r N_b\left(\frac{1}{2m^4} + \frac{h^2}{6m^2} - \frac{h^4}{60}\right) - \frac{G_r N_b(N_b^2+N_t^2)}{36864}\left(\frac{7372800h}{m^{10}} + \frac{921600h^3}{m^8} + \frac{37248h^5}{m^6} + \frac{624h^7}{m^4} + \frac{7h^{11}}{24}\right) - \frac{B_r N_t}{N_b}\left(\frac{h}{2m^2} - \frac{h^3}{16}\right) + B_r N_t\left(\frac{1}{2m^4} + \frac{h^2}{6m^2} - \frac{h^4}{60}\right) + \frac{B_r(N_b^2+N_t^v)}{36864}\frac{N_t}{N_b}\left(\frac{1152h}{m^6} + \frac{144h^3}{m^4} + \frac{6h^5}{m^2} - \frac{3h^7}{8}\right)\right)\right]$$

4. RESULT AND ANALYSIS

The pressure drop, resistance of the flow, and wall shear stress are denoted by Equations (33), (36) and (39 & 40), respectively. The impact of various flow characteristics on flow resistance and wall shear stress have been studied by considering the parameter values as $d_1 = 0.2, d_2 = 0.2, L_1 = 0.2, L_2 = 0.2, L = 1,\ N = 0.1, q = 0.3, F = 0.3, B_r = 0.3, G_r = 0.2, N_b = 0.3, N_t = 0.8, \alpha = \pi/6, k = 0.05$. (Prasad, K. M., & Sudha, T. [43]).

Figures (2-10) depict the impact of various parameters on flow resistance ($\bar{\lambda}$) for various values of stenoses (δ_1) and dilatation heights (δ_2), inclination ($\emptyset$), Thermophoresis parameter (N_t), Local Nanoparticle Grashof number (B_r), Brownian motion number (N_b), local temperature Grashof number (G_r), Viscosity (μ), Permeability of Porous medium (k) and Magnetic parameter (M).

From the Figures (2-10), it is observed that when the height of the stenosis (δ_1) increases the resistance of the flow increases and height of the dilatation (δ_2) increases the flow resistance decreases.

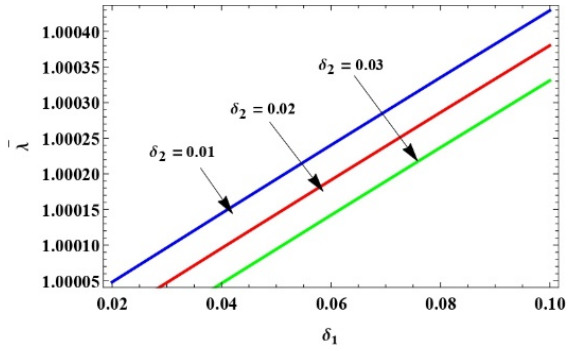

Figure. 2. Variation of $\bar{\lambda}$ with for δ_1 varying of δ_2

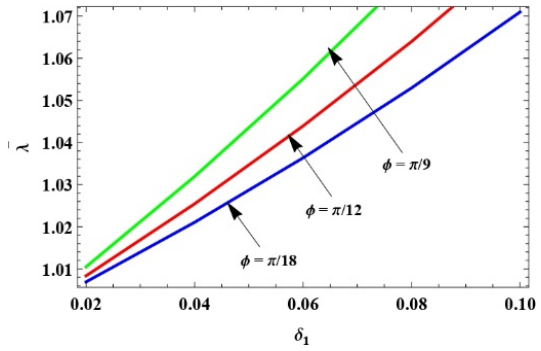

Figure 3. Variation of $\bar{\lambda}$ with for δ_1 varying of $\emptyset$

It is also observed from the Figures (2-10) that, the flow resistance ($\bar{\lambda}$) increases with Inclination ($\emptyset$), Local Nanoparticle Grashof number (B_r), Magnetic Parameter (M) and Viscosity (μ) and the flow resistance ($\bar{\lambda}$) decreases

with thermophoresis parameter (N_t), Brownian motion parameter (N_b), Local Temperature Grashof number (G_r) and Permeability of Porous medium (k).

From the Fig. 5 and Fig. 8, it is interesting to observe that the flow resistance increases with increasing of Local Nanoparticle Grashof number (B_r) and viscosity (μ). Because of variation in temperature, buoyancy forces become more significant than viscous forces, influencing flow behaviour. Whereas buoyancy increases fluid motion, the combined impacts of viscosity and nanoparticle interactions contribute to increased flow resistance.

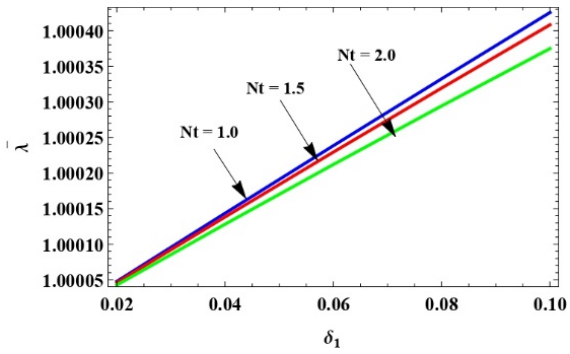

Figure.4. Variation of $\bar{\lambda}$ with for δ_1 varying of N_t

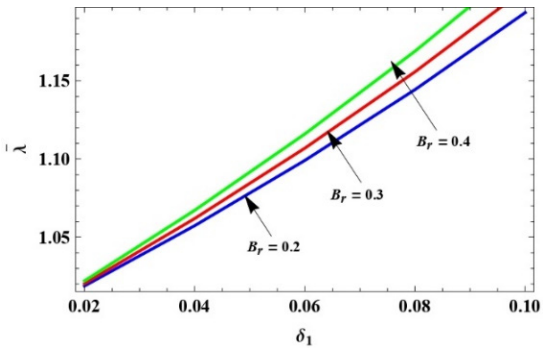

Figure. 5. Variation of $\bar{\lambda}$ with for δ_1 varying of B_r

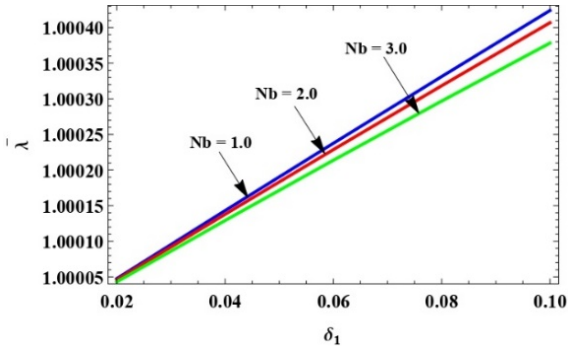

Figure. 6. Variation of $\bar{\lambda}$ with for δ_1 varying of N_b

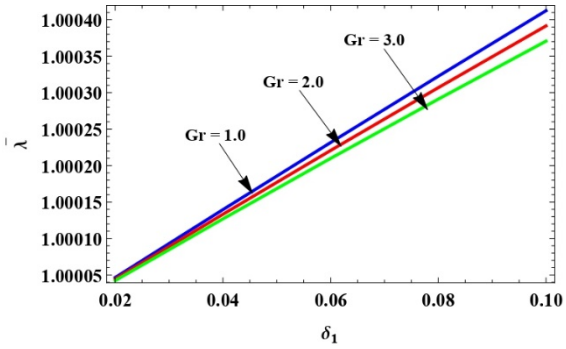

Figure. 7. Variation of $\bar{\lambda}$ with for δ_1 varying of G_r

From the Fig. 9, it is interested to notice that the impedance to the flow increases with stenosis height (δ_1) and permeability (k) this increase is significant when stenosis height(δ_1) exceeds the value 0.03. i.e in small arteries, the permeability effect is less than plaque deposition.

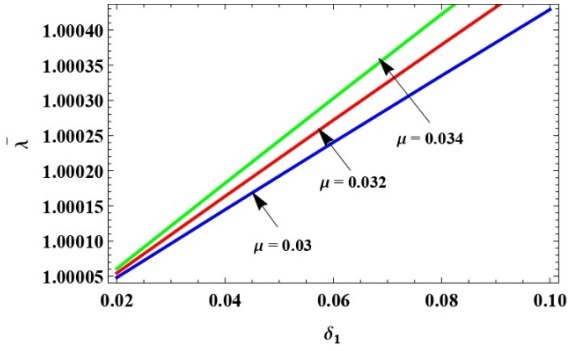

Figure. 8. Variation of $\bar{\lambda}$ with for δ_1 varying of $\boldsymbol{\mu}$

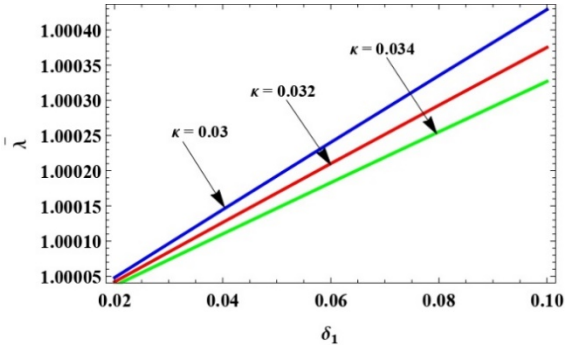

Figure. 9. Variation of $\bar{\lambda}$ with for δ_1 varying of k

From the Fig. 10, it is interesting to observe that the flow resistance increases with increase in magnetic parameter (M), However it is noticed that this increase is only significance when the stenosis height (δ) exceeds the value 0.03.

A magnetic field applied perpendicular to the flow interacts with charged nanoparticles, causing a drag force that reduces the fluid and increases flow resistance. However, by controlling the magnetic field appropriately, it becomes possible to control blood pressure and improve conditions such as poor circulation

Nanoparticles in a fluid strengthen the thermal properties by enhancing molecular collisions, however they also introduce increased flow resistance. Temperature fluctuations produce buoyancy effects, defined by the local nanoparticle Grashof number, while the permeability of porous medium affects blood flow efficiency. In systems such as vascular networks and drug delivery devices, the optimization of blood flow can be obtained through systematic adjustment of these parameters.

Figures (11-19) demonstrate the effect of velocity profiles for various values of Brownian motion number (N_b), Magnetic parameter (M), Local temperature Grashof number (G_r), micropolar parameter (m), local nanoparticle Grashof number (B_r), Permeability of porous medium (k), Thermophoresis parameter (N_t), Viscosity (μ) and Inclination ($\emptyset$).

It is noted that from the Figures (11-19) the velocity profiles increase with the increase of local nanoparticle Grashof number (B_r), Permeability of porous medium (k) and Thermophoresis parameter (N_t), but decreases with the increasing of brownian motion parameter (N_b), Local temperature Grashof number (G_r), Micropolar parameter (m), Viscosity (μ) and Inclination ($\emptyset$).

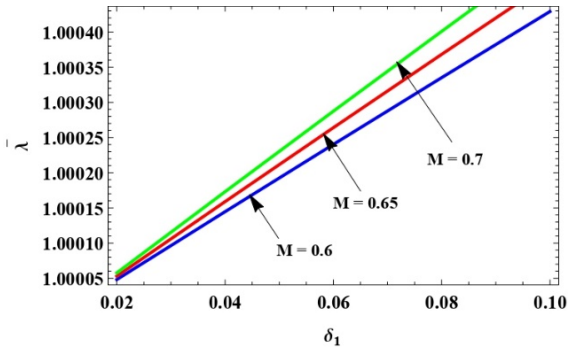

Figure 10. Variation of $\bar{\lambda}$ with for δ_1 varying of M

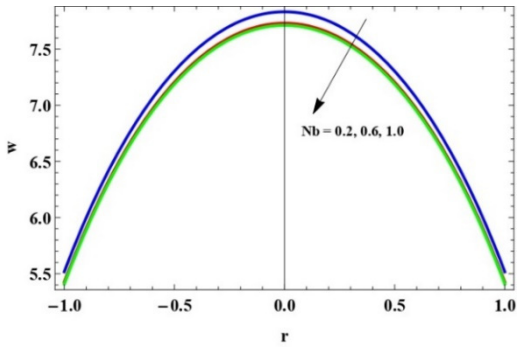

Figure 11. Variation of $\boldsymbol{w}$ with. $\boldsymbol{N_b}$

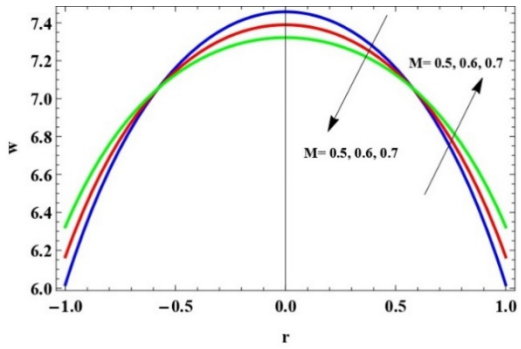

Figure 12. Variation of $\boldsymbol{w}$ with $\boldsymbol{M}$

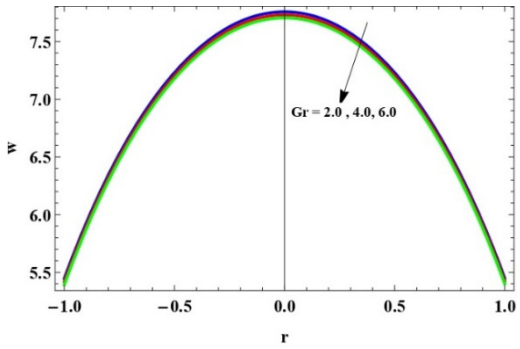

Figure 13. Variation of $\boldsymbol{w}$ with $\boldsymbol{G_r}$

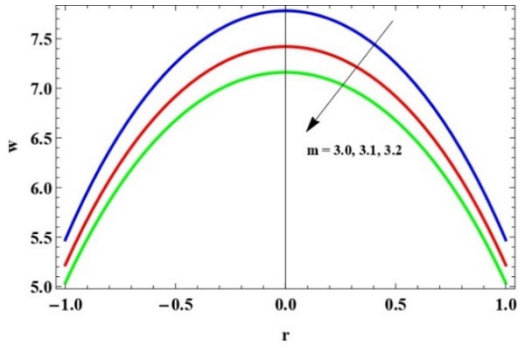

Figure 14. Variation of $\boldsymbol{w}$ with $\boldsymbol{m}$

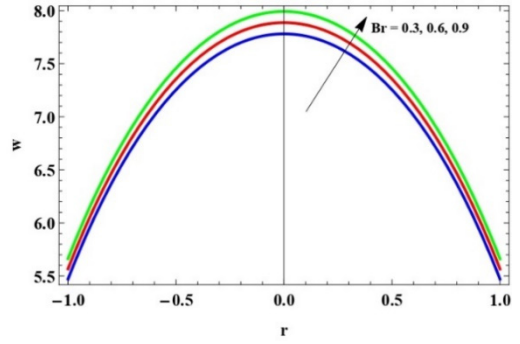

Figure 15. Variation of $\boldsymbol{w}$ with $\boldsymbol{B_r}$

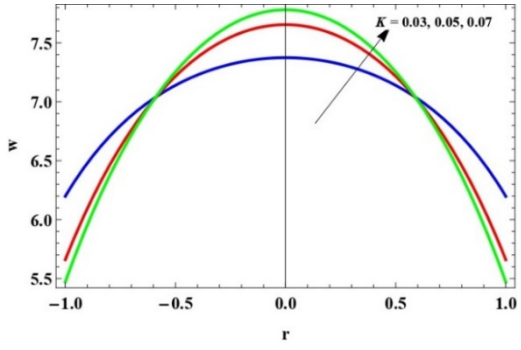

Figure 16. Variation of $\boldsymbol{w}$ with $\boldsymbol{k}$

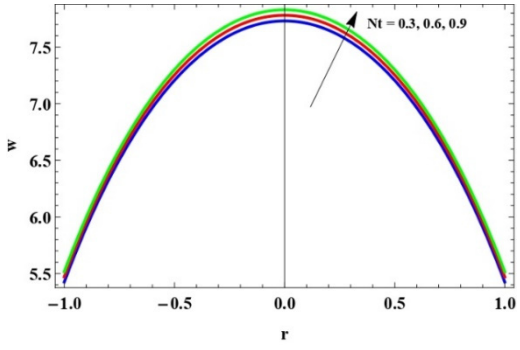

Figure 17. Variation of $\boldsymbol{w}$ with $\boldsymbol{N_t}$

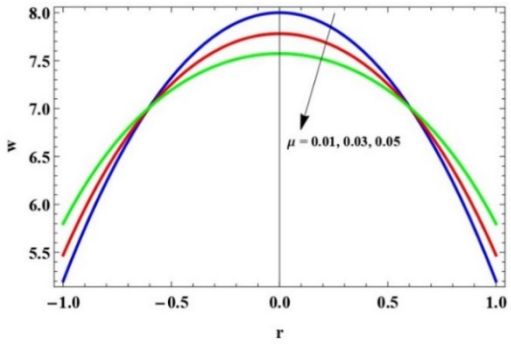

Figure 18. Variation of $\boldsymbol{w}$ with $\boldsymbol{\mu}$

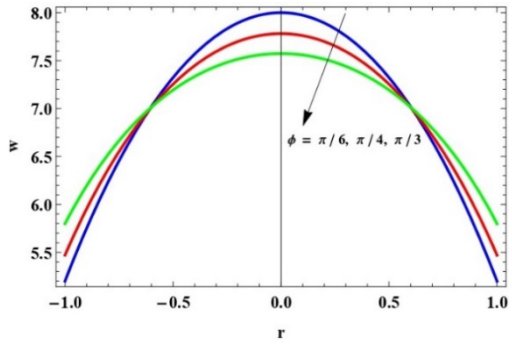

Figure 19. Variation of $\boldsymbol{w}$ with $\emptyset$

From the Fig. 12. It is interesting to identified that, the effect velocity profile decreases in the range of −0.5 to 0.5 with an increase of magnetic parameter (M) is and increasing in the other region.

Figures (20-37) demonstrate the variations of wall shear stress (τ_{rz} & τ_{zr}) versus z are shown to understand the progression of arterial disorders with various flow parameters for various values of micropolar parameter (m), Magnetic parameter (M), Brownian motion number (N_b), local temperature Grashof number (G_r), Thermophoresis parameter (N_t), Local Nanoparticle Grashof number (B_r), Viscosity (μ), Inclination $(\emptyset)$ and Permeability of Porous medium (k)

It is noticed that from the Figures (20-37) micropolar parameter (m), Magnetic parameter (M), Brownian motion parameter (N_b), local temperature Grashof number (G_r), Thermophoresis parameter (N_t), and Local Nanoparticle Grashof number (B_r) Inclination $(\emptyset)$, Permeability of Porous medium (k) decrease with the wall shear stress.

Increasing magnetic field effect, which produce a Lorentz force that decreases the flow momentum. Consequently, wall shear stress values decrease along z at every position.

The viscosity(μ), thermophoresis parameter (N_t), and magnetic parameter (M) all lead to the minimized wall shear stress, which is favourable in systems where excessive shear stress may be harmful. This is particularly relevant in delicate microfluidic devices and the human circulatory system, where maintaining optimal shear stress is required to minimize tissue injury and provide effective fluid flow.

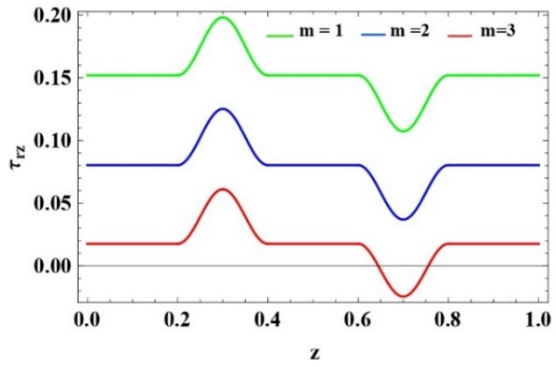

Figure 20. Variation of z on τ_{rz} with m varying

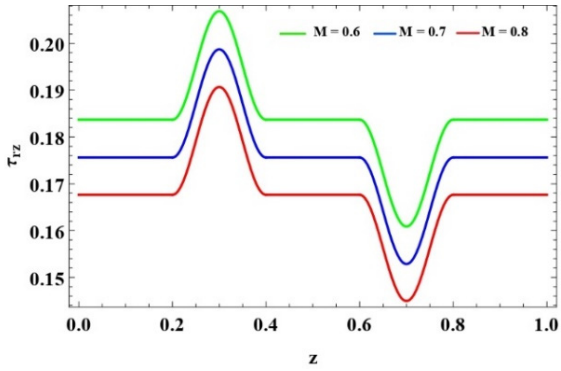

Figure 21. Variation of $\boldsymbol{z}$ on $\boldsymbol{\tau_{rz}}$ with $\boldsymbol{M}$ varying

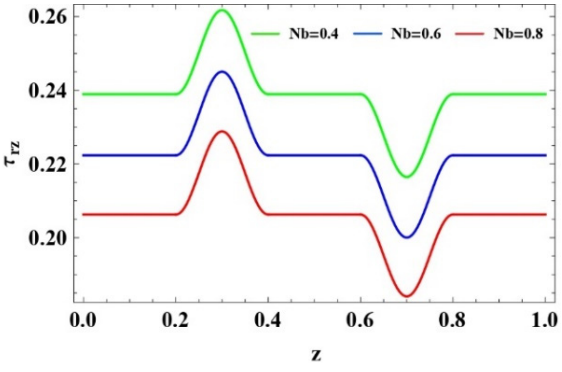

Figure 22. Variation of z on τ_{rz} with N_b varying

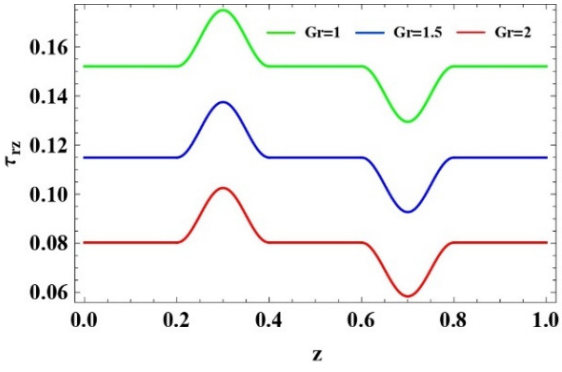

Figure 23. Variation of z on τ_{rz} with G_r varying

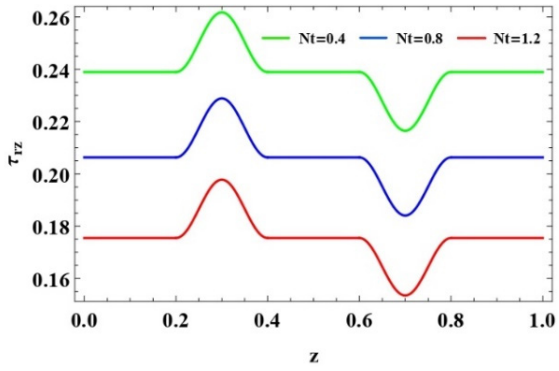

Figure 24. Variation of z on τ_{rz} with N_t varying

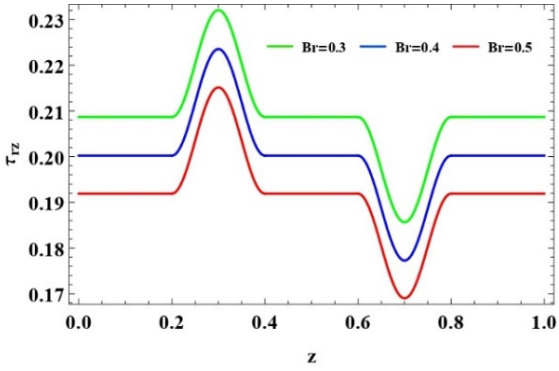

Figure 25. Variation of z on τ_{rz} with B_r varying

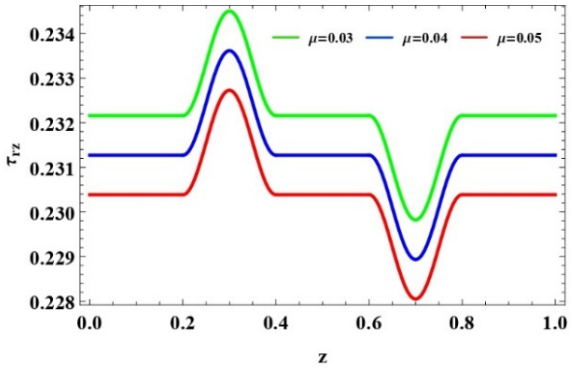

Figure 26. Variation of z on τ_{rz} with μ varying

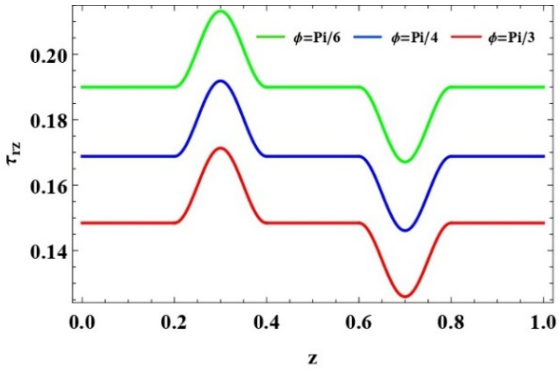

Figure 27. Variation of z on τ_{rz} with ∅ varying

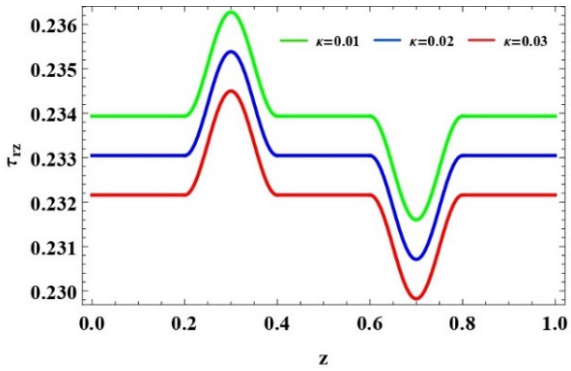

Figure 28. Variation of $\boldsymbol{z}$ on $\boldsymbol{\tau_{rz}}$ with $\boldsymbol{k}$ varying

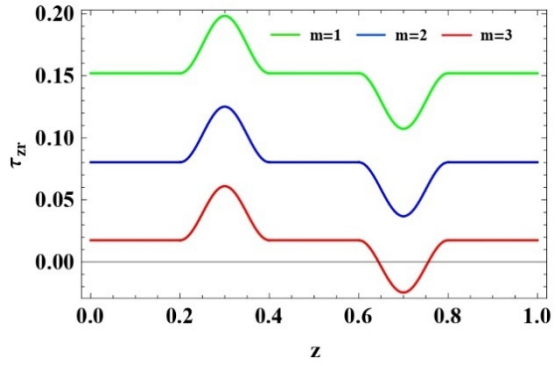

Figure 29. Variation of $\boldsymbol{z}$ on $\boldsymbol{\tau_{zr}}$ with $\boldsymbol{m}$ varying

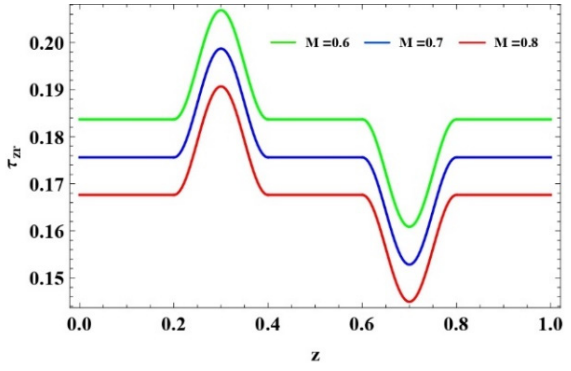

Figure 30. Variation of $\boldsymbol{z}$ on $\boldsymbol{\tau_{zr}}$ with $\boldsymbol{M}$ varying

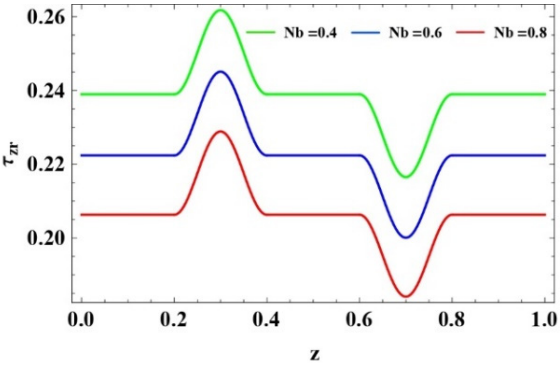

Figure 31. Variation of $\boldsymbol{z}$ on $\boldsymbol{\tau_{zr}}$ with $\boldsymbol{N_b}$ varying

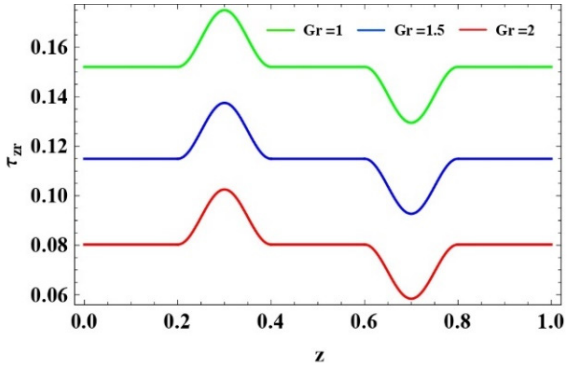

Figure 32. Variation of z on τ_{zr} with G_r varying

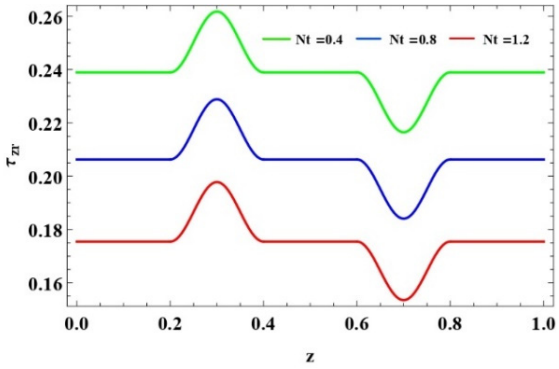

Figure 33. Variation of z on τ_{zr} with N_t varying

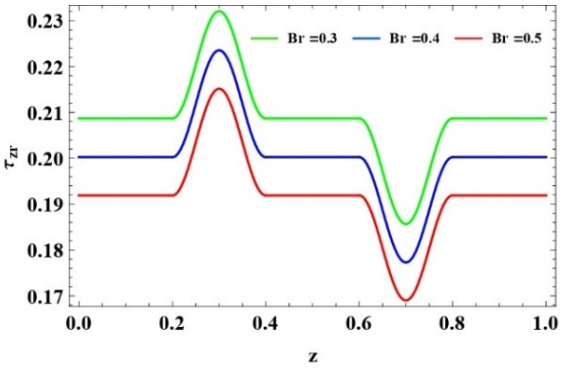

Figure 34. Variation of z on τ_{zr} with B_r varying

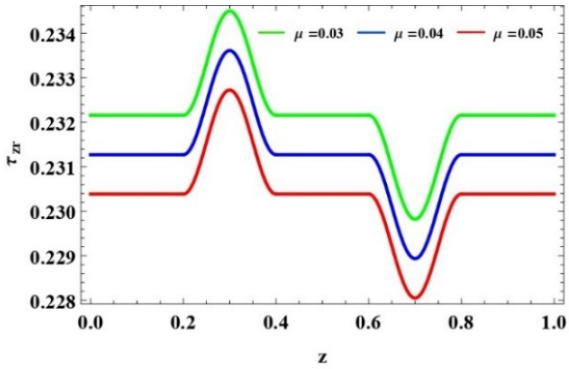

Figure 35. Variation of z on τ_{zr} with μ varying

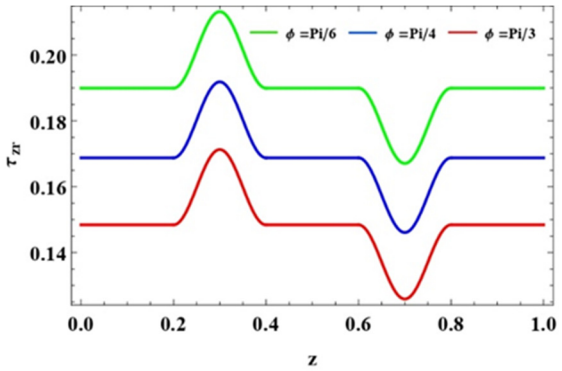

Figure 36. Variation of z on τ_{zr} with ∅ varying

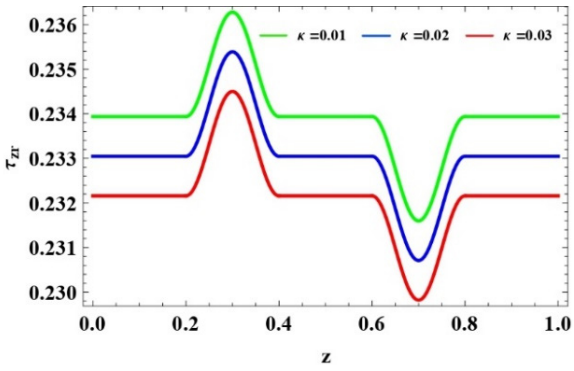

Figure 37. Variation of z on τ_{zr} with k varying

Figures (38-40) displays the streamlines for various values of k, M *and* B_r , It has been seen that the stream lines are getting closure with increase of k, M *and* B_r. It is seen that, the streamlines in the middle are becoming widen, it shows that the blood velocity is increasing and these reduces the resistance to flow decreases with the increase in values of k, M.

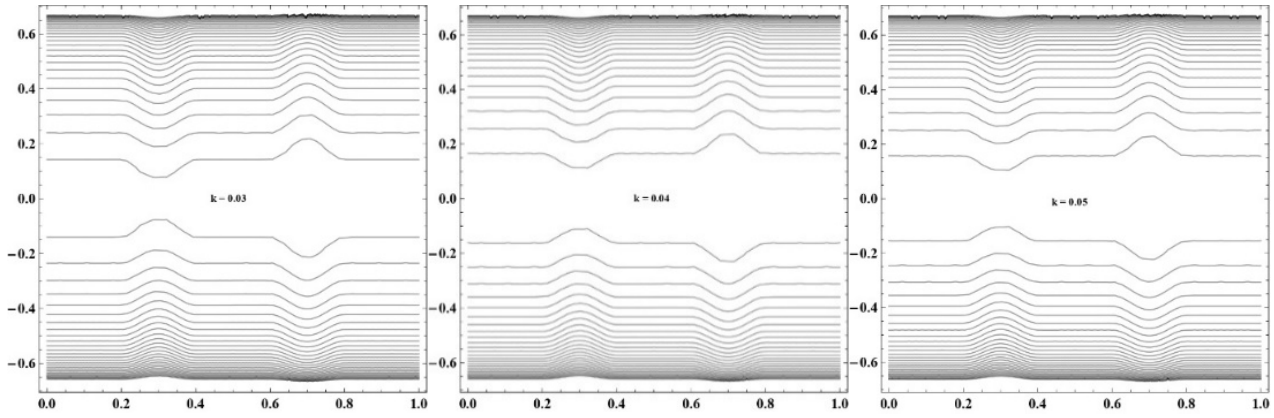

Figure 38. Streamlines for $k = 0.03, 0.04$ *and* 0.05

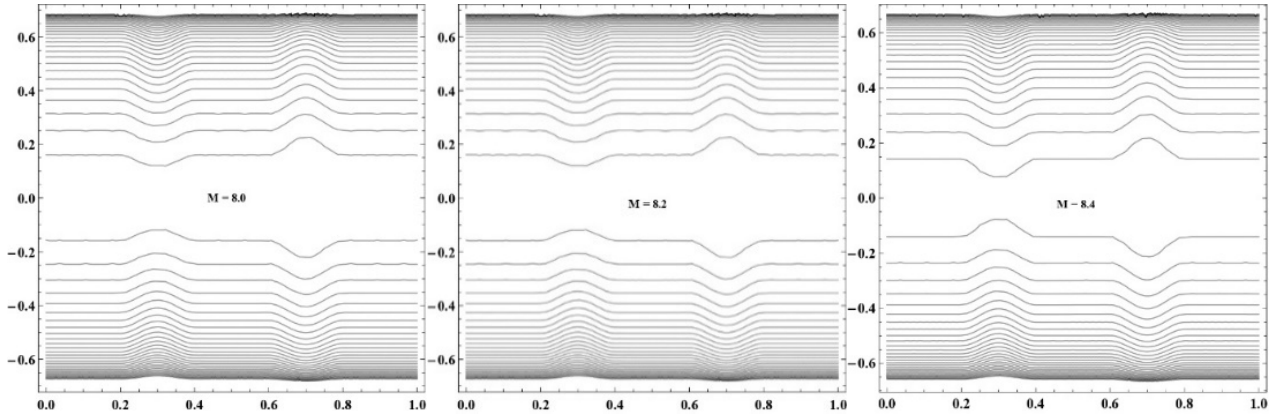

Figure 39. Streamlines for $M = 8.0, 8.2 \; and \; 8.4$

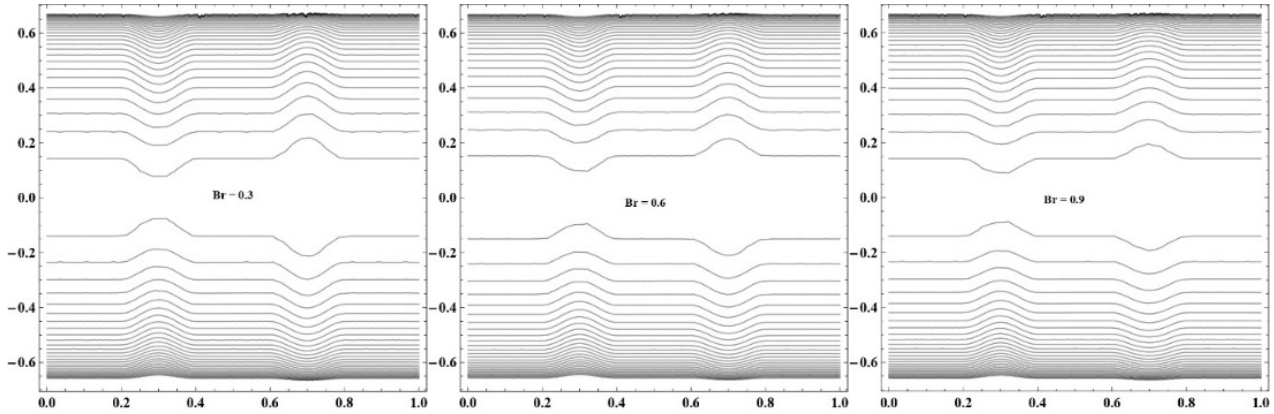

Figure 40. Streamlines for $B_r = 0.3, 0.6 \; and \; 0.9$

5. CONCLUSIONS

The influence of magnetic field on a micropolar fluid through an inclined porous medium with multiple abnormal segments has been studied. It was possible to evaluate the impact of various factors with different stenosis heights on the flow impedance and shear stress at the wall by finding solutions to the flow characteristic expressions.

The Observations are:

- Magnetic Parameter, Inclination, Local Nanoparticle Grashof number and Viscosity increases with flow resistance.
- The heights of stenotic dilatation, Thermophoresis parameter, Permeability of Porous medium, Local Temperature Grashof number and Brownian motion parameter decreases with the flow resistance.
- The resistance of the flow and shear stress at the wall decreasing for the values of heights of the stenosis dilatation
- It is identified that the effect of velocity profile with the increase of magnetic parameter (M) is decreasing in the region -0.5 to 0.5 and increasing in the other region.
- The heights of stenotic dilatation, Magnetic Parameter, Brownian motion number, Inclination, Local Temperature Grashof number, Thermophoresis parameter, Local Nanoparticle Grashof number and Permeability of Porous medium decreases with the shear stress at the wall.
- Study on micropolar nanofluids improves understanding of blood's microstructure and particle behaviour in magnetic fields. Incorporating micropolarity, magnetic effects, and nanoparticle dynamics (such Brownian motion and thermophoresis) improves the accuracy of blood flow models, especially for arterial stenosis or dilatation. These advanced simulations can enhance the design of medical devices such as stents and blood pumps, enable more precise targeted drug delivery systems, and support advanced diagnostic tools that simulate pathological blood flow conditions.
- The study demonstrates that blood flow resistance and wall shear stress in stenosed and dilated arteries are influenced by important factors such magnetic field strength, nanoparticle dynamics, and arterial geometry. Significantly, these results have direct applications in hematology and biomedical engineering. Controlling the external magnetic field can be used to optimize treatment techniques for cardiovascular disorders such as hypertension, atherosclerosis, and arterial blockages by regulating blood flow and shear stress.
- The streamlines lines are getting closure with the increase of Permeability of Porous medium, Magnetic parameter, Local Nanoparticle Grashof number.

ORCID
Narender Satwai, https://orcid.org/0000-0003-1466-4556; **K. Maruthi Prasad,** https://orcid.org/0000-0002-9010-6452

REFERENCES

[1] D.F. Young, "Effect of a time dependent stenosis of flow through a tube," Journal of Engineering for Industry, **90**(2), 248-254 (1968). https://doi.org/10.1115/1.3604621
[2] J.B. Shukla, R.S. Parihar and B.R.P. Rao, "Effects of stenosis on non-newtonian flow of the blood in an artery," Bulletin of Mathematical Biology, **42**(3), 283–294 (1980). https://doi.org/10.1016/s0092-8240(80)80051-6
[3] J.-S. Lee and Y.-C. Fung, "Flow in Locally Constricted Tubes at Low Reynolds Numbers," Journal of Applied Mechanics, **37**(1), 9–16 (1970). https://doi.org/10.1115/1.3408496
[4] P. Chaturani and R.P. Samy, "Pulsatile flow of Casson's fluid through stenosed arteries with applications to blood flow," Biorheology, **23**(5), 499–511 (1986). https://doi.org/10.3233/bir-1986-23506
[5] G. Radhakrishnamacharya and S. Rao, "Flow of a magnetic fluid through a non-uniform wavy tube," Proceedings of the National Academy of Sciences, India. Section A. Physical Sciences, 77, (2007).
[6] D.F. Young and F.Y. Tsai, "Flow characteristics in models of arterial stenosis-I: steady flow," Journal of Biomechanics, **6**, 395-410 (1973). https://doi.org/10.1016/0021-9290(79)90004-6
[7] K.M. Prasad and P.R. Yasa, "Micropolar fluid flow in tapering stenosed arteries having permeable walls," Malaysian Journal of Mathematical Sciences, **15**(1), 147–160 (2021).
[8] D.J. Schneck and S. Ostrach, "Pulsatile blood flow in a channel of small exponential divergence-I. The linear approximation for low mean Reynolds number," J. Fluids Eng. **16**, 353–360 (1975). https://doi.org/10.1115/1.3447314
[9] K.M. Prasad and G. Radhakrishnamacharya, "Effect of multiple stenoses on Herschel–Bulkley fluid through a tube with non-uniform cross-section," International e-journal of engineering mathematics: Theory and Application, 1, 69–76 (2007).
[10] A.C. Eringen, "Theory of micropolar fluids," Journal of Mathematics and Mechanics, **16**(1), 1–18 (1966). https://www.jstor.org/stable/24901466
[11] G.R. Charya, "Flow of micropolar fluid through a constricted channel," In International Journal of Engineering Science, **15**(12), 719–725 (1977). https://doi.org/10.1016/0020-7225(77)90022-2
[12] T. Ariman, M.A. Turk, and N. Sylvester, "Application of microcontinum fluid mechanics," Int. J. Eng. Sci. **12**, 273–293 (1974). http://dx.doi.org/10.1016/0020-7225(74)90059-7
[13] K.M. Prasad, B. Sreekala and P.R. Yasa, "Analysis of micropolar fluid with nanoparticles flow through a core region in a stenosed artery having mild stenoses," Palestine Journal of Mathematics, **12**(4) (2023).
[14] D. Srinivasacharya, M. Mishra and A. Rao, "Peristaltic pumping of a micropolar fluid in a tube," Acta Mechanica, **161**, 165–178 (2003). https://doi.org/10.1007/s00707-002-0993-y
[15] K.M. Prasad and P.R. Yasa, "Flow of non-Newtonian fluid through a permeable artery having non-uniform cross section with multiple stenosis," Journal of Naval Architecture and Marine Engineering, **17**(1), 31–38 (2020). https://doi.org/10.3329/jname.v17i1.40942
[16] E. Yeom, Y.J. Kang and S.J. Lee, "Changes in velocity profile according to blood viscosity in a microchannel," Biomicrofluidics, **8**, 034110 (2014). https://doi.org/10.1063/1.4883275
[17] E. Karvelas, G. Sofiadis, T. Papathanasiou and I. Sarris, "Effect of micropolar fluid properties on the blood flow in a human carotid model," Fluids, **5**(3), 125 (2020).
[18] S.U.S. Choi and J.A. Eastman, "Enhancing thermal conductivity of fluids with nanoparticles," in: *ASME International Mechanical Engineering Congress & Exposition*, (San Francisco, United States, 1995).
[19] Noreen Sher Akbar and S. Nadeem, "Peristaltic Flow of a Micropolar Fluid with Nanoparticles in Small Intestine," Applied Nanoscience, **3**(6), 461-468 (2013). https://doi.org/10.1007/s13204-012-0160-2
[20] S. Nadeem and S. Ijaz, "Theoretical analysis of metallic nanoparticles on blood flow through stenosed artery with permeable walls," Physics Letters A, **379**(6), 542-554 (2015). https://doi.org/10.1016/j.physleta 2014.12.013
[21] A.M. Abd-Alla, E.N. Thabet and F.S. Bayones, "Numerical solution for MHD peristaltic transport in an inclined Nano fluid symmetric channel with porous medium," Sci. Rep. **12**(1), 1-11 (2022). https://doi.org/10.1038/s41598-022-07193-5
[22] J. He, N.S. Elgazery, K. Elagamy and A.N.Y. Elazem, "Efficacy of a modulated viscosity-dependent temperature/nanoparticles concentration parameter on a nonlinear radiative electromagnetic-Nano fluid flow along an elongated stretching sheet," J. Appl. Comput. Mech. **9**(3), 848-860 (2023). https://doi.org/10.22055/jacm. 2023 42294.3905
[23] K. Prasad, Y. Prabhaker and A.R. Mohammed, "Thermal effects of two immiscible fluids through a permeable stenosed artery having nanofluid in the core region," Heat Transfer, **51**(5), 4562-4583 (2022). https://doi.org/10.1002/htj.22513
[24] K.M. Prasad, N. Subadra, P.R. Shekhar and R.B. Vijaya, "Jeffrey fluid flow driven by peristaltic pumping with nanoparticles in an inclined tube," Journal of Naval Architecture & Marine Engineering, **20**(2), 165–175 (2023). https://doi.org/10.1002/htj.22513N
[25] A.S. Dawood, F.A. Kroush, R.M. Abumandour, and I.M. Eldesoky, "Multi-effect analysis of nanofluid flow in stenosed arteries with variable pressure gradient: analytical study," SN Applied Sciences, **5**(12), 382 (2023). https://doi.org/10.1007/s42452-023-05567-6
[26] Md.A. Ikbal, S. Chakravarty, K.K.L. Wong, J. Mazumdar and P.K. Mandal, "Unsteady response of non-Newtonian blood flow through a stenosed artery in magnetic field," In Journal of Computational and Applied Mathematics, **230**(1), 243–259 (2009). https://doi.org/10.1016/j.cam.2008.11.010
[27] R. Bali and U. Awasthi, "Effect of a magnetic field on the resistance to blood flow through stenotic artery," Applied Mathematics and Computation, **188**(2), 1635–1641 (2007). https://doi.org/10.1016/j.amc.2006.11.019
[28] J.C. Misra, A. Sinha and G.C. Shit, "Mathematical modelling of blood flow in a porous vessel having double stenoses in the presence of an external magnetic field," International Journal of Biomathematics, **04**(02), 207–225 (2011). https://doi.org/10.1142/s1793524511001428

[29] J.-H. He, "A coupling method of a Homotopy technique and a perturbation technique for non-linear problems," In International Journal of Non-Linear Mechanics, **35**(1), 37–43 (2000). https://doi.org/10.1016/s0020-7462(98)00085-7
[30] J.-H. He, "Application of homotopy perturbation method to nonlinear wave equations," Chaos, Solitons & Fractals, **26**(3), 695–700 (2005). https://doi.org/10.1016/j.chaos.2005.03.006
[31] I.J.D. Craig and P.G. Watson, "Magnetic reconnection solutions based on a generalized Ohm's law," Solar Phys. **214**, 131–150 (2003). https://doi.org/10.1023/A:1024075416016
[32] V.K. Sud, G.S. Sephon and R.K. Mishra, "Pumping action on blood flow by a magnetic field," Bull. Math. Biol. **39**, 385 (1977). https://doi.org/10.1007/BF02462917
[33] H.L. Agrawal and B. Anwaruddin, "Peristaltic flow of blood in a branch," Ranchi Univ. Math. J. **15**, 111–121 (1984).
[34] T. Sochi, "Non-Newtonian flow in porous media," Polymer, **51**(22), 5007–5023 (2010). https://doi.org/10.1016/j.polymer.2010.07.047
[35] K.M. Prasad and P.R. Yasa, "Mathematical Modelling on an Electrically Conducting Fluid Flow in an Inclined Permeable Tube with Multiple Stenoses," International Journal of Innovative Technology and Exploring Engineering, **9**(1), 3915–3921 (2019). https://doi.org/10.35940/ijitee.a4989.119119
[36] W.F.W. Azmi, A.Q. Mohamad, L.Y. Jiann and S. Shafie, "Mathematical fractional analysis on blood Casson fluid in slip and small arteries with the cholesterol porosity effect," Malaysian Journal of Mathematical Sciences, **18**(4), 755–774 (2024). https://doi.org/10.47836/mjms. 18.4.05
[37] K.M. Prasad, and P.R. Yasa, "Flow of non-Newtonian fluid through a permeable artery having non-uniform cross section with multiple stenosis," Journal of Naval Architecture and Marine Engineering, **17**(1), 31–38 (2020). https://doi.org/10.3329/jname.v17i1.40942
[38] T. Sudha, C. Umadevi, M. Dhange, S. Manna, and J.C. Misra, "Effects of stenosis and dilatation on flow of blood mixed with suspended nanoparticles: A study using Homotopy technique," **26**(1), 251-265 (2021). https://doi.org/10.2478/ijame-2021-0015
[39] M.K. Prasad, R.B. Vijaya and C. Umadevi, "Effects of Stenosis and Post Stenotic Dilatations on Jeffrey Fluid Flow in Arteries," International Journal of Research in Engineering and Technology, **4**, 195-201 (2015). https://doi.org/10.15623/ijret.2015.0413032
[40] B. Pincombe, B. Mazumdar, and J. Hamilton-Craig, "Effects of multiple stenoses and post- stenotic dilation on non- Newtonian blood flow in small arteries," Medical & Biological Engineering & Computing, **37**(5), 595–599 (1999). https://doi.org/10.1007/bf02513353
[41] M. Dhange, G. Sankad, R. Safdar, W. Jamshed, M.R. Eid, U. Bhujakkanavar, *et al*., "A mathematical model of blood flow in a stenosed artery with post-stenotic dilatation and a forced field," PLoS ONE, **17**(7), e0266727 (2022). https://doi.org/10.1371/journal.pone.0266727
[42] K.M. Prasad, N. Subadra and M.A.S. Srinivas, "Peristaltic transport of a micropolar fluid with nanoparticles in an inclined tube with permeable walls," International Journal of Advanced Research Trends in Engineering and Technology (IJARTET), **4**(10), (2017). https://ijartet.com/2750/v4i10/journal
[43] K.M. Prasad and T. Sudha, "The effects of post-stenotic dilatations on the flow of micropolar fluid through stenosed artery with suspension of nanoparticles," AIP Conference Proceedings, **2246**(1), 020082 (2000). https://doi.org/10.1063/5.0014455

МОДЕЛЮВАННЯ МГД ПОТОКУ МІКРОПОЛЯРНОЇ НАНОРИДИНИ В ПОХИЛІЙ ПОРИСТІЙ СТЕНОЗОВАНІЙ АРТЕРІЇ З ДИЛАТАЦІЄЮ

Нарендер Сатвай[a,b], Каранаму Маруті Прасад[a]

[a]*Кафедра математики, Школа наук, GITAM (Вважається університетом), Хайдерабад, штат Телангана, Індія – 502329*
[b]*Кафедра математики, Технологічний інститут Б. В. Раджу, Вішнупур, Нарсапур, штат Телангана, Індія – 502313*

У цій статті досліджується вплив магнітного поля на кровотік з частинами нанорідини через похилу пористу стенозовану артерію та дилатацію. Тут кров розглядається як мікрополярна рідина. Рівняння розв'язуються за допомогою методу гомотопічних бурень [HPM] у припущенні легкого стенозу. Отримано розв'язки замкнутої форми швидкості, профілю температури та розподілу концентрації. Спостерігався вплив відповідних параметрів на явища потоку, а результати аналізуються графічно. Це дослідження розглядає вплив магнітного параметра на характеристики потоку та показує, що наявність магнітного поля збільшує опір потоку, одночасно зменшуючи напруження зсуву на стінці. В результаті виявлено, що опір потоку та напруження зсуву на стінці зменшується з високою дилатацією стенозу. Крім того, дослідження показує, що опір потоку збільшується, а напруження зсуву на стінці зменшується зі збільшенням в'язкості. Лінії потоку побудовані для вивчення картини потоку та властивостей передачі імпульсу.

Ключові слова: *стеноз; дилатація; мікрополярна рідина; опір потоку; напруження зсуву на стінці; параметр броунівського руху; параметр термофорезу*